SPATIAL GROWTH PATTERNS OF *PSEUDOMONAS AERUGINOSA* BIOFILMS

by

Ruifang Xu

A thesis submitted in partial fulfillment
of the requirements for the degree

of

Master of Science

in

Chemical Engineering

MONTANA STATE UNIVERSITY
Bozeman, Montana

July 2004

APPROVAL

of a thesis submitted by

Ruifang Xu

This thesis has been read by each member of the thesis committee and has found to be satisfactory regarding content, English usage, format, citations, bibliographic style, and consistency, and is ready for submission to the College of Graduate Studies.

Dr. Philip S. Stewart

Approved for the Department of Chemical and Biological Engineering

Dr. Ron Larsen

Approved for the College of Graduate Studies

Dr. Bruce R. McLeod

STATEMENT OF PERMISSION OT USE

In presenting this thesis in partial fulfillment of the requirements for a master's degree at Montana State University, I agree that the Library shall make it available to borrowers under rules of the Library.

If I have indicated my intention to copyright this thesis by including a copyright notice page, copying is allowable only for scholarly purposes, consistent with "fair use" as prescribed in the U.S. Copyright Law. Requests for permission for extended quotation from or reproduction of this thesis in whole or in parts may be granted only by the copyright holder.

Signature: RUIFANG XU

Date: 07/19/2004

ACKNOWLEDGMENTS

I could not have completed my Master of Science degree in Chemical Engineering without the nice people I met at the Montana State University. First and foremost, I must thank Dr. Phil Stewart for being a wonderful advisor for my research. In addition, I want to thank Dr. Michael Franklin and Dr. James Duffy for revising my thesis. Also, I would like to acknowledge all the members in the Control lab for all the kind help and friendship. And, thank you to all the people of the Center for Biofilm Engineering for the friendship.

Finally, I would like to thank my parents. They are always supporting me.

TABLE OF CONTENTS

LIST OF TABLES

LIST OF FIGURES

ABSTRACT

Biofilms are less susceptible to antimicrobial action compared to their planktonic counterparts. The protective mechanisms are not fully understood. Physiological heterogeneity within biofilms is thought to contribute to the low susceptibility and was therefore studied. Expression of green fluorescent protein (GFP), induction of alkaline phosphatase (APase) by phosphate starvation, and the cell viability assay using the LIVE/DEAD *Bac*Light bacterial viability stain were performed to visualize the spatial patterns of growth and viability within 5-d-old *Pseudomonas aeruginosa* biofilms.

The capillary reactor and the drip-flow reactor were employed to obtain biofilms of a range of thickness. Biofilms cultivated in the capillary reactor were usually thinner than those grown in the low-shear drip-flow reactor. The former were examined by in situ confocal scanning laser microscopy (CSLM) whereas the latter were cryoembedded and cryosectioned prior to conventional fluorescence microscopic observation.

P. aeruginosa PAO1 with the plasmid pAB1 carrying an inducible, stable *gfp* was used to identify zones of active protein synthesis. The induction of *gfp* proved suitable for the visualization of spatial growth patterns within biofilms. Greater GFP activity was evident at the surface of clusters and was not as bright in their centers after induction. Activity appeared more uniform in smaller clusters and less uniform in larger clusters. The APase activity induced by phosphate starvation showed a sharply delineated band of active APase synthesizing cells close to the biofilm-bulk fluid interface and some local APase synthetic activity in the depth of the biofilm. The results of biofilm viability staining using the LIVE/DEAD *Bac*Light bacterial viability kit turned out to be puzzling and cast doubt on the methodological validity of applying the LIVE/DEAD *Bac*Light bacterial viability staining method to *P. aeruginosa* biofilms.

The findings of the spatial growth patterns illustrate the physiological heterogeneity that is present in these biofilms. Such variation in the metabolic activity probably contributes to the reduced susceptibility of these biofilms to antimicrobial agents.

CHAPTER 1

INTRODUCTION

Biofilm Physiology

The physiology of biofilm cells is extremely complex and is profoundly different from those grown planktonically. It is generally believed that the attachment of microbes to a solid surface can influence their metabolic activities in a way that is not easily predicted on the basis of current knowledge (Anwar *et al.* 1992). The physiological status of biofilm cells is heterogeneous and is determined by the location of each individual cell within the multiple layers of cells that form the biofilm. Cells located in the upper regions of the biofilm (surface biofilm cells) may have easy access to nutrients, including oxygen, and have fewer problems with the discharge of metabolic waste products. These cells are metabolically active. The cell envelopes are likely to be permeable to nutrients. The surface biofilm cells are likely to have properties very similar to their planktonic counterparts. In contrast, cells enmeshed within the thick glycocalyx matrix (embedded biofilm cells) are likely to be less metabolically active because of poor access to essential nutrients, including oxygen. These cells also have problems associated with the accumulation of waste metabolites in their surroundings. Embedded biofilm cells are at

the stage of dormancy, and these cells are likely to be smaller than the surface biofilm cells since they are not actively engaged in cell division. The formation of biofilms, however, generates a sheltered encapsulated community of cells in which environmental stresses are greatly reduced (Anwar *et al.*, 1992).

Biofilm Resistance

Largely as a result of the failures to properly use and monitor antibiotic therapy, almost all pathogenic microorganisms have developed resistance to some chemotherapeutic agents since widespread use of antimicrobial chemotherapy began in the 1950s. Some multi-drug resistant strains of *Pseudomonas aeruginosa* are now even untreatable with known antimicrobial drugs (Madigan *et al.*, 2003). Furthermore, bacteria attached to surfaces aggregate in a hydrated polymeric matrix of their own synthesis to form biofilms, and biofilm bacteria predominate, numerically and metabolically, in virtually all nutrient-sufficient ecosystems. Therefore, these sessile organisms predominate in most of the environmental, industrial, and medical problems and processes of interest to microbiologists. Biofilm organisms differ significantly in physiology from planktonic organisms, most notably with respect to the low susceptibility of biofilm organisms to antibiotics and disinfectants. Formation of these sessile communities and their inherent resistance to antimicrobial agents are at the root of

many persistent and chronic bacterial infections (Costerton *et al.* 1995; McLean and Decho, 2002).

Reduced susceptibility was frequently observed in ubiquitous bacterial biofilms. Treatment of an infection after biofilm is established is frequently futile with current remedies (Costerton *et al.*, 1999). The low susceptibility of undesired biofilms constitutes a threat to industry and human health. Although resistance mechanisms are important to combat the recalcitrance of biofilms, they are not completely revealed yet.

Mechanisms for Reduced Susceptibility of Biofilms to Antimicrobial Action

Many hypotheses have been developed to explain the reduced susceptibility of biofilms to antibiotics. All these are probably closely related to the structural and chemical heterogeneity of the biofilms. It is structural and chemical heterogeneities that distinguish biofilm microorganisms from their planktonic counterparts and confer the reduced susceptibility to biofilms. Structural heterogeneity was termed as the feature as non-uniform distribution of cells and polymers within the biofilm matrix and variable biofilm thickness (Murga *et al.*, 1994). Chemical heterogeneity, indicated by the local variation in the concentrations of metabolic substrates, products, and microbial species, is another one of the hallmarks of the biofilm mode of growth. Concentration profiles for oxygen, nitrite, nitrate, ammonium, pH, sulfide, and methane in biofilms have been

experimentally measured (Stewart, 2003). Sternberg *et al.* (1999), Wentland *et al.* (1996) and Xu *et al.*, (1998) used GFP expression, alkaline phosphatase induction, acridine orange staining to visualize and quantify spatial variations in growth rate within biofilms, respectively. It was concluded that the slow and spatially heterogeneous growth of microorganisms within biofilms surely results from such gradients of nutrients (including oxygen).

Penetration limitation and physiological limitation were commonly hypothesized to result in the heterogeneous growth patterns and thus contribute to the protective mechanisms of biofilms.

Penetration Limitation

One explanation for the biofilm resistance mechanisms is that only the upper layers of a biofilm near the biofilm-bulk fluid interface are exposed to the attack by a lethal dose of antibiotic due to a reaction-diffusion barrier that limits penetration of the antibiotic into the biofilm. Diffusion is the predominant transport process within cell aggregates (de Beer *et al.*, 1997; Stoodley *et al.*, 1994). A mathematical theory was developed to investigate the antibiotic penetration into microbial biofilm. The reaction-diffusion mechanism was supposed to be a viable explanation for failure of certain antibiotics to control biofilm infections (Stewart, 1996). Anderl *et al.* have evaluated the significance of penetration limitation as a mechanism of *Klebsiella pneumoniae* biofilm resistance to

two antibiotics, ampicillin and ciprofloxacin. Poor penetration contributed to wild-type *K. pneumoniae* biofilm resistance to ampicillin but not to ciprofloxacin. The increased resistance of the wild-type strain to ciprofloxacin and the mutant strain to ampicillin and ciprofloxacin could not be accounted for by antibiotic inactivation or slow diffusion since these antibiotics fully penetrated the biofilm. These results suggested that some other resistance mechanism is involved for both antimicrobial agents (Anderl *et al.*, 2000).

Physiological limitation

Physiological limitation refers to changes in the nutrient or growth status of cells in a biofilm that could contribute to reduced susceptibility to antibiotics. The roles of various physiological factors, such as growth rate, biofilm age, starvation, and oxygen limitation have long been studied.

The oxygen distribution was thought to be strongly correlated with the complex structures consisting of microbial cell clusters (discrete aggregates of densely packed cells) and interstitial voids (de Beer *et al.*, 1994). Borriello *et al.* (2004) produced a profile of oxygen distribution within the *P. aeruginosa* biofilms using oxygen microelectrodes. They related the biofilm susceptibility to oxygen limitation and concluded that while oxygen deprivation protected *P. aeruginosa*, it did not reduce susceptibility in short-term cultures to the same low levels measured for 48-h colony biofilms in most cases. When the log reductions for mature colony biofilms were

compared with the log reductions for young biofilms under anaerobic conditions, oxygen limitation could account for as much as 62 to 100% of the protection, depending on the agent. This suggested that oxygen limitation is one of the important factors in the tolerance of *P. aeruginosa* biofilms to killing by antibiotics, but it is probably not the only factor.

Shigeta *et al.* (1997) and Tanaka *et al.* (1999) evaluated the effect of the growth rate of biofilm of leucine-requiring mutant *P. aeruginosa* HU1 cells on their susceptibility to antimicrobial agents, three β-lactams and several fluoroquinolones. It was suggested that the bactericidal action of some antibiotics such as β-lactams against biofilm cells is affected by the cell growth rate, while the bactericidal action of fluoroquinolones is considerably greater and independent on the growth rate.

Wentland *et al.* (1996) used acridine orange to visualize and quantify the spatial variations in growth rate within *K. pneumoniae* colonies and biofilms. Bacteria were indicated to grow rapidly near the biofilm-bulk fluid interface and grow slowly in the biofilm interior.

Huang *et al.* (1966) and Xu *et al.* (1998) studied the physiological change occurring to the *P. aeruginos*a biofilms after exposure to phosphate starvation by determining the spatial pattern of de novo alkaline phosphatase synthetic activity. They found a sharply delineated band expressing alkaline phosphatase activity along the biofilm-bulk fluid interface and almost no alkaline phosphatase expressed elsewhere. The consistence of the spatial heterogeneity of alkaline phosphatase expression with the oxygen profile inside

the biofilms they revealed further supported the hypothesis of oxygen limitation against that of glucose limitation.

Objectives

The overall goal of this work was to determine the spatial growth patterns of *P. aeruginosa* biofilms and examine the spatial viability pattern to help reveal the physiological heterogeneity of these biofilms.

The specific objectives were:

Objective 1. To visualize the growth rate-dependent green fluorescent protein synthetic activity (Chapter 2, 3).

Rationale: *gfp* gene had been used as a marker to monitor the gene expression and protein localization in *Escherichia coli* culture on plates and in first-stage *Caenorhabditis elegans* larvae, etc. However, prior to the beginning of this research, very little work was aimed at employing the inducible *gfp* gene to reveal the spatial physiological heterogeneity of protein synthetic activity in the *P. aeruginosa* biofilms.

Objective 2. To visualize the phosphate starvation-induced alkaline phosphatase expression in the *P. aeruginosa* biofilms (Chapter 4).

Rationale: Revealing the influence of phosphate starvation on the physiological heterogeneity of alkaline phosphatase expression in biofilms would provide information to study the biofilm resistance to antimicrobial agents.

Objective 3. To visualize the spatial viability pattern in these biofilms using LIVE/DEAD *Bac*Light bacterial viability kit (Chapter 5).

Rationale: LIVE/DEAD *Bac*Light bacterial viability assay was widely applied to the bacterial suspension cultures whereas very little work was done to study the biofilm viability pattern.

Pseudomonas aeruginosa PAO1 (pAB1) Strain and Media

P. aeruginosa is a ubiquitous environmental bacterium found in almost every ecological niche, including soil, water, and plants and is an opportunistic pathogen initiating infections in individuals whose resistance is low. It is a gram-negative organism capable of forming biofilms on surfaces as a survival strategy (Deziel *et al.*, 2001; Madigan *et al.*, 2003). The cells of *P. aeruginosa* respond to favorable nutrient conditions by adhering to available surfaces and by binary fission and exopolymer production to develop mature biofilms (Costerton *et al.*, 1995). The initiation of biofilm formation in *P. aeruginosa* was shown to be correlated with the emergence of hyperpiliated and highly adherent phenotypic variants that are deficient in swimming, swarming, and twitching

motilities. (Moat *et al.*, 2002). These rod-shaped vegetative cells (0.8×1.2 μm) grow predominantly in the matrix-enclosed sessile mode of growth, in which they are protected from adverse environmental conditions and from biological and chemical antibacterial agents (Costerton *et al.*, 1995).

In the present work, *P. aeruginosa* PAO1 strain carrying an inducible plasmid pAB1, which was constructed by Franklin, M. J., was studied (Franklin and Ohman, 1996; Figurski and Helinski, 1979; Franklin and Ohman, 1993; Nivens *et al.*, 2001; Franklin *et al.*, 1994; Walters *et al.*, 2003).

A minimal glycerol-glutamate medium, Keck project medium (Table 1.1) was used to grow the *P. aeruginosa* biofilms.

Table 1.1. Keck project medium for *P. aeruginosa* growth

Ingredient	Formula	Concentration (g/L)
Glutamic Acid (sodium salt)	$C_5H_8NO_4Na$	0.1522
Glycerol	$C_3O_3H_8$	0.4605
Magnesium Sulfate	$MgSO_4$-$7H_2O$	0.0493
Sodium Phosphate Monobasic	NaH_2PO_4-$2H_2O$	0.2340
Potassium Phosphate Dibasic	K_2HPO_4	0.5922
Sodium Chloride	NaCl	8.4738

pH value adjusted to 7.
Note: to make the Keck project medium agar plates, add 15 g/L Bacto™ agar to the Keck project medium.

There are two pathways through which *P. aeruginosa* is known to be able to grow anaerobically: denitrification or fermentation of arginine. Thus, in an anaerobic environment, in the absence of nitrate, nitrite and arginine, the growth and metabolism of *P. aeruginosa* are completely arrested (Borriello *et al.*, 2004). To test the specific viability of the *P. aeruginosa* PAO1 (pAB1) strain on the Keck project medium in aerobic and anaerobic environments, the strain was streaked onto the Keck project medium agar plates and then incubated. After 2 d of aerobic growth at ambient temperature (23^{o}C), tiny colonies showed up, which was indicative of the initiation of growth. At the end of the third day, colonies were larger. It showed that the *P. aeruginosa* cells could grow on the Keck project medium under aerobic conditions. However, if incubated for 5 d under anaerobic conditions inside an anaerobic pouch, no colonies were visible on the Keck project medium agar plate. The plate was taken out of the pouch and transferred to the ambient aerobic environment. After 2 d of aerobic growth, colonies appeared the same as they did in standard aerobic growth. It showed that cells can survive, but not grow, on the Keck project medium under anaerobic conditions without supply of nitrate, nitrite or arginine (data not shown).

CHAPTER 2

SPATIAL GROWTH PATTERNS OF *PSEUDOMONAS AERUGINOSA* CAPILLARY REACTOR BIOFILMS VISUALIZED BY USING AN INDUCIBLE GREEN FLUORESCENT PROTEIN

Introduction

The advent of fluorescent proteins has created an ideal tool for the direct microscopic examination of biological activities in biofilms. The green fluorescent protein (GFP), coded by the *gfp* gene, which encodes a 238-amino acid-residue polypeptide (Prasher *et al.*, 1992), absorbs blue light (maximally at 395 nm with a minor peak at 470 nm) and emits green light (peak emission at 509 nm with a shoulder at 540 nm) (Figure 2.1). This green fluorescence is very stable and can be detected by fluorescence microscopy (Chalfie *et al.*, 1994).

GFP has strong visible absorbance and fluorescence from a p-hydroxybenzylidene-imidazolidinone chromophore, which is generated by cyclization and oxidation of the protein's own Ser-Tyr-Gly sequence at positions 65-67. It was reported that formation of the final fluorophore requires molecular oxygen and proceeds with a time constant (≈ 4 h

at 22 ^{o}C and atmospheric pO_2) independent of dilution, implying that the oxidation does not require enzymes or cofactors. (Heim *et al.*, 1994)

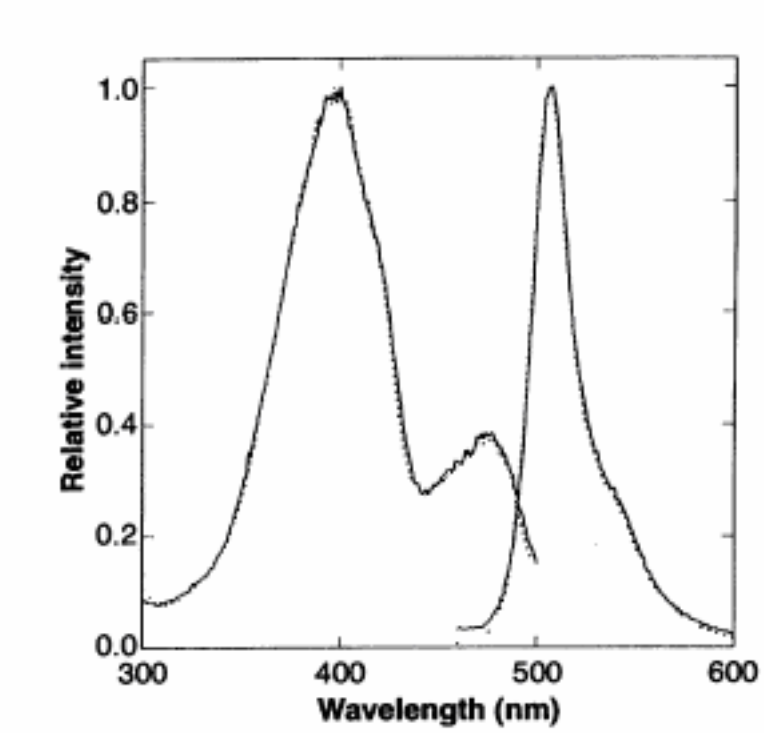

Figure 2.1. Excitation and emission spectra of GFP (Chalfie *et al.*, 1994)

Sternberg *et al.* have studied the cellular growth activity in *Pseudomonas putida* biofilms using a strain carrying the *rrn*BP1-*gfp* (AAV) fusion as a useful marker. Since these variant GFP have considerably shorter half-lives than wild-type GFP and can thus be rapidly degraded, the strain provides online monitoring of changes from high to low bacterial activity. In contrast, the control strain in their work carried *rrn*BP1 fused to the stable *gfp*mut3b* gene, a reduction in activity (or signal intensity) could not be detected in colonies comparable in size. Similarly, an isopropyl β-D-thiogalactopyranoside

(IPTG)-inducible *gfp* gene construct was employed as an indicator to map the spatial patterns of the protein synthetic activity in the biofilms of *P. aeruginosa* in the present work because only those actively growing cells capable of protein synthesis could be induced with IPTG to express GFP. GFP expression would be turned off if the cells ceased growing. That blocked the accumulation of synthesized GFP, which thus correlated the growth rate to the protein synthesis rate and made a real-time visualization of the spatial growth patterns of *P. aeruginosa* biofilms. A strain carrying a constitutively expressed *gfp*mut2 gene was used as a control.

Materials and Methods

Strains, Plasmids and Media

P. aeruginosa PAO1 strain with the plasmid pAB1, carrying an IPTG-inducible, stable *gfp*, was used in this study. The strain was constructed by Franklin, Michael J. The plasmid pAB1 was stably maintained in *P. aeruginosa*. Carbenicillin at a final concentration of 50 μg/ml was added into the medium. The strain was grown in a minimal glycerol-glutamate medium, Keck project medium (Table 1.1). Medium was prepared and adjusted to pH 7.0 prior to autoclaving.

The plasmid pAB1 contained the *lacI* repressor and therefore induction of the *gfp* could be controlled through the addition of IPTG to the medium (Walters *et al.*, 2004). Considering the cells growth in the continuous presence of the inducer, GFP did not appear to have a toxic effect on the cells. In the *P. aeruginosa* PAO1 (pAB1) stain, because the detection of intracellular GFP required only irradiation by near UV or blue light, it was not limited by the availability of substrates other than oxygen, which was required for the formation of the final fluorophore, and IPTG. Thus, the inducible *gfp* should provide an excellent means for monitoring gene expression and protein localization in living cells (Chalfie *et al.*, 1994).

As described in Figure 2.2, growing cells with active GFP synthetic activity and the presence of IPTG and oxygen are required for GFP expression in the biofilms of *P. aeruginosa* PAO1 (pAB1). Bright green fluorescence develops in those *P. aeruginosa* PAO1 (pAB1) cells that are actively synthesizing protein in the presence of the IPTG and oxygen. The more active the growth, the greater the GFP expression. In the absence of either IPTG or oxygen, the *P. aeruginosa* PAO1 (pAB1) cells will not be induced and no green fluorescence will be observed.

Since the plasmid pMF230 does not contain the *lacI* repressor, *gfp* is expressed constitutively. *P. aeruginosa* PAO1 (pMF230) was used as a control strain.

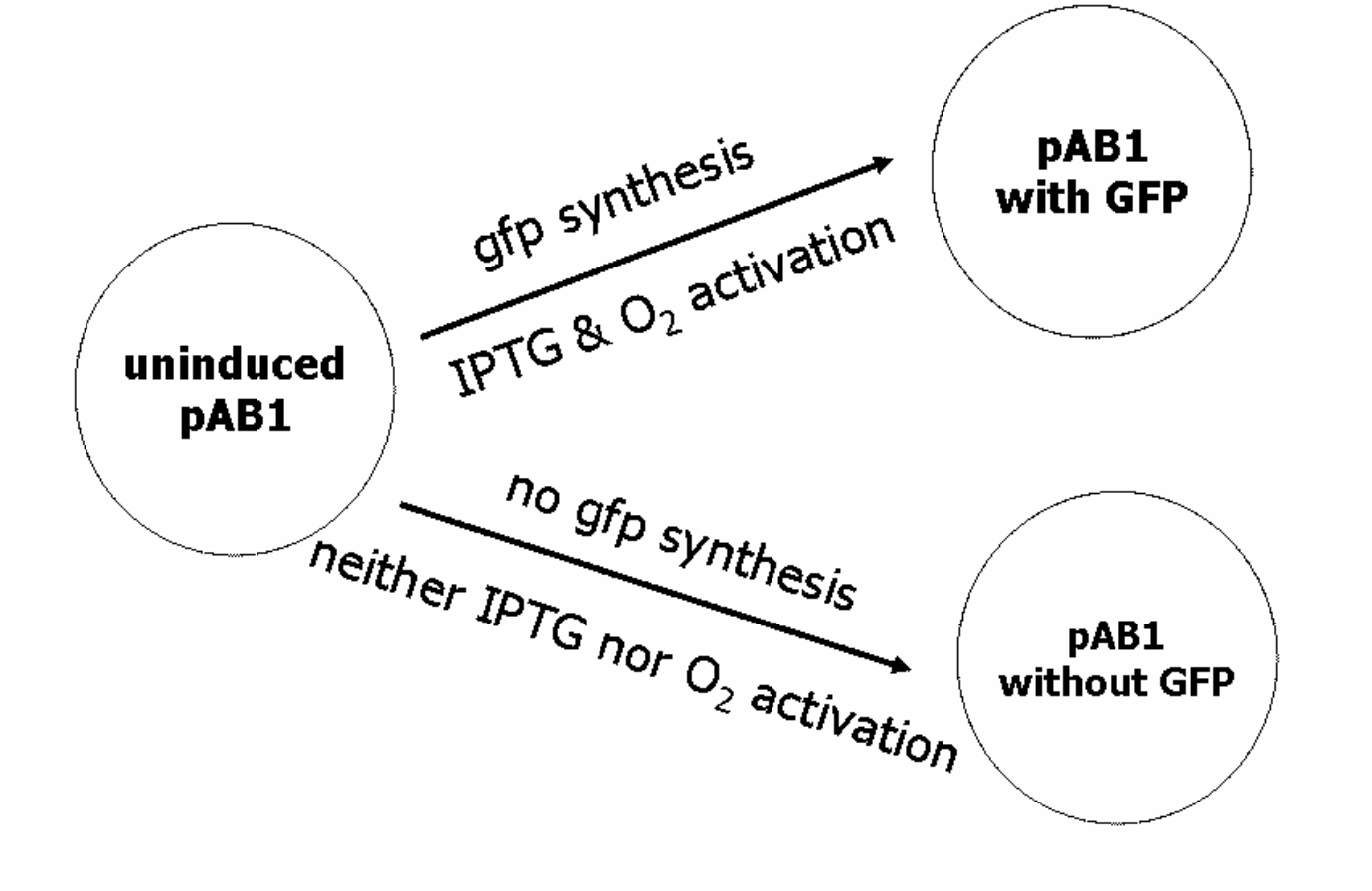

Figure 2.2. Reactions within the *P. aeruginosa* PAO1 cell with pAB1 plasmid which carries an IPTG-inducible stable *gfp* gene

Capillary Reactor System

Biofilms were grown in glass capillary tube under continuous laminar flow conditions. The glass tube was special ordered from Friedrich & Dimmock, Inc (Millville, New Jersey; www.fdglass.com). It had a nominal inside dimension of 900 μm and a square cross section with a wall thickness of 0.17 ± 0.1 mm, allowing in situ microscopic examination of biofilms growing on the inside of the tube through the flat tube wall. Due to its fragility, the capillary was positioned in a flow cell holder to reduce the chance of breakage. The apparatus consisted of a vented medium feed carboy (4 liter capacity), a flow break, a filtered air entry, a peristaltic pump, the capillary and flow cell holder, two inoculation ports (one upstream of the capillary, named inoculation port #1, the other downstream of the capillary, named inoculation port #2), and a waste carboy. All components were connected by silicone rubber tubing. The flow cell holders were special ordered from Biosurface Technologies in Bozeman, Montana.

We discovered enhanced development of biofilm cell clusters of *P. aeruginosa* by pumping air through the capillary along with the liquid medium. Air was pumped at the same flow rate as the medium, 20 ml/h, using parallel tubes through the same peristaltic pump, which made the biofilms physically stronger, perhaps caused by the increased shear force and additional oxygen supply. The air and medium flows were mixed in a T-connector just downstream of the pump and upstream of the glass capillary. This resulted in slug flow of medium and air bubbles through the capillary tube.

The schematic of the capillary reactor system and set-up is shown in Figure 2.3.

Cultivation Procedure

P. aeruginosa biofilms were grown for 5 d in the Keck project medium at ambient temperature (23 ^{o}C). The remaining reactor components were plumbed and autoclaved separately. Working in a laminar flow hood after allowing hot items to cool, the medium carboy was connected to the rest of the apparatus. The system was removed from the hood to the laboratory bench and then filled with liquid medium as a final check for leaks prior to inoculation.

With the pump off, the tubing was clamped downstream of inoculation port #2. About 2 ml of an overnight culture of the PAO1 (pAB1) strain (optical density at 600 nm of 0.001 to 0.005) was stained by red food color and inoculated via inoculation port #2 upstream to fill the glass capillary. The tubing upstream of the glass tube was clamped when the red food color indicated the medium flow through the glass capillary. The system was then allowed to stand in no flow conditions for 24 h, which facilitated the attachment of bacteria to the interior surface of the capillary.

The clamps were removed and medium flow was initiated at a flow rate of 20 ml h^{-1}. The biofilm was allowed to grow under the laminar flow conditions for 5 d.

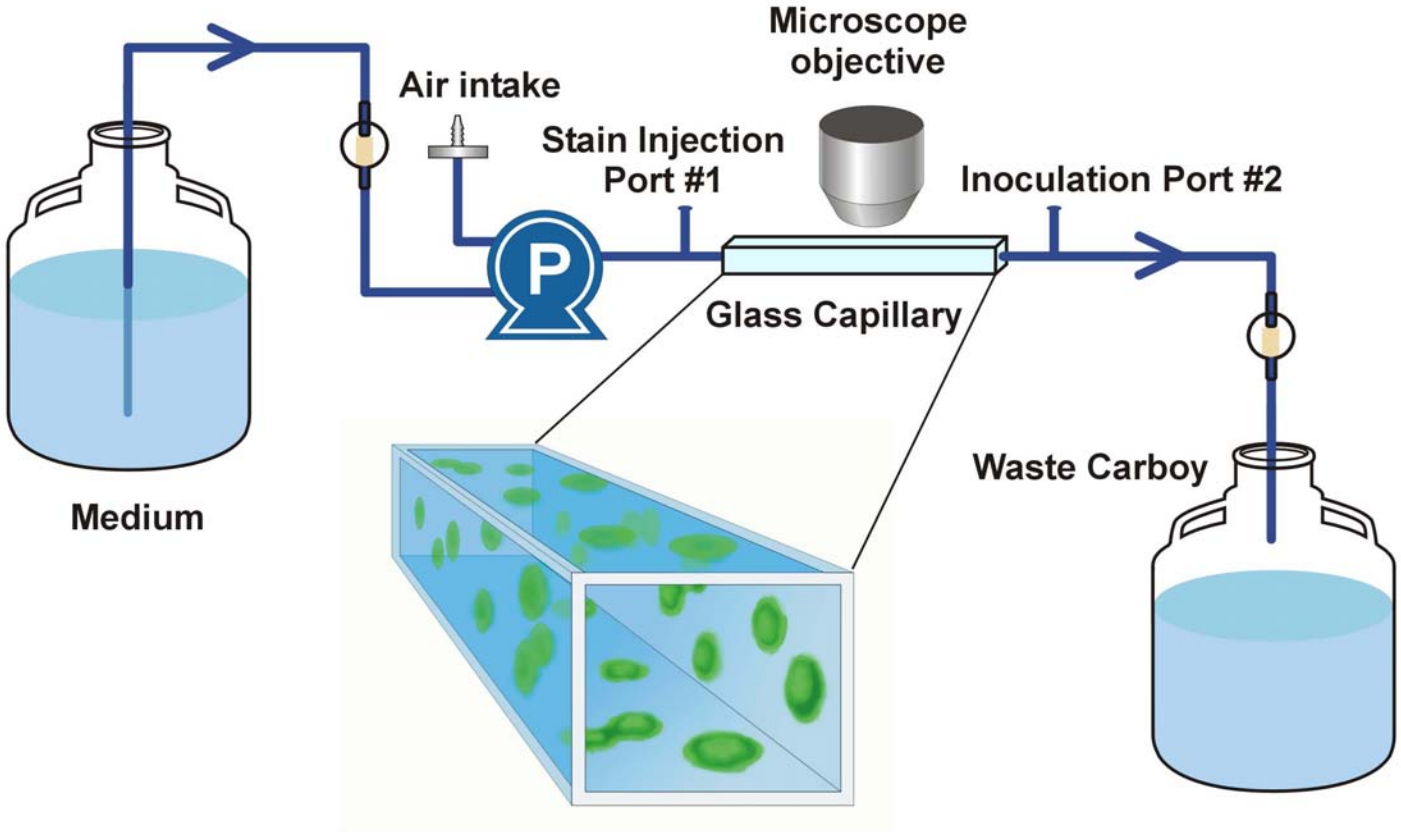

Figure 2.3. Schematic of capillary reactor system used to grow *P. aeruginosa* PAO1 (pAB1) biofilms

Microscopic Examination

After 5 d of growth, the *P. aeruginosa* biofilms matured and were ready for in-situ microscopic examination. The reactor system was moved to the confocal scanning laser microscopy (CSLM) facility and the glass capillary placed on the microscope stage in its holder.

Coincident with the beginning of microscopic examination, the inducer IPTG was fed continuously at a final concentration of 1 mM along with the medium to the biofilm. A time-lapse movie over a period of 3 h after IPTG addition was taken to visualize the temporal pattern of *gfp* expression during the 3 h of IPTG addition.

To better interpret the spatial patterns of GFP activity in these biofilms, counterstaining by rhodamine B chloride was employed. Rhodamine B chloride (Tetraethylrhodamine), $C_{28}H_{31}ClN_2O_3$ (MW 479.02), with the excitation peak at λmax of 540 nm and emission peak at 625 nm, was used as the best complementary stain for GFP. With the pump off, the tubing was clamped upstream of stain injection port #1. About 5 ml of 50 mg/ml rhodamine B solution was injected via stain injection port #1 downstream to counterstain the biofilm inside the glass capillary. The staining solution was allowed to stand in the capillary for 5 min. At which time, the clamps were removed and medium flow initiated to rinse the stain. The biofilm sample in the capillary was then prepared for observation.

The excitation peak of rhodamine B is around 540 nm, emission peak around 625 nm. A Leica TCS-NT equipped with an argon 488-nm laser for GFP fluorescence excitation, a krypton 568-nm laser for rhodamine B fluorescence excitation, a DD488/568 dichroic beam splitter, and a BP525/50 emission filter for GFP (green) and a BP 600/30 emission filter for rhodamine B (red) (or Leica TCS-SP2 AOBS which uses the acousto-optical beam splitter instead of filters and mechanical beam splitters to sort the emission light) was applied to collect the microscopic images. A 10× or 20× or 40× water immersion or dry lens was used.

CLSM allows in situ analysis of biofilms. This feature, coupled with the ability to digitally extract optical thin sections from specific biofilm locations, free from out-of-focus optical interference, permits the direct examination of complex *xy* and *xz* spatial and chemical relationships that exist between bacteria, their extracellular products, and their environment (Wilson, 1990), which greatly favors microscopic examination of the samples without refocusing all the time.

Image Analysis by MetaMorph Software

Images of single slices at specific heights (Z-position) can be easily obtained. Z-series image stacks were made by collecting the images of single slices all through the thickness of the biofilm cluster, which could be combined to reconstruct the 3-dimensional structure and visualize the growth patterns of the biofilm sample.

Time-lapse movies were made by scanning a single plane at a specific Z-position repeatedly over a period to study the temporal patterns of the microbial activities, in this case GFP expression.

Quantitative analysis of the confocal images was performed using the built-in Linescan function of MetaMorph image analysis software. The fluorescence intensity of the biofilms was quantified by measuring the gray levels of the images. Linear transects of various widths were set across the biofilm clusters to test the intensity of the fluorescence from the synthesized GFP along the lines, either located at different spots on a spatial basis to map the spatial growth patterns of the GFP synthetic activity or located at a specific region on a temporal basis to study the temporal growth patterns.

Results

Under transmission imaging, a plan view of the spatial structure and biomass distribution of the *P. aeruginosa* biofilm inside the capillary revealed rounded cell clusters (Figure 2.4).

In order to better interpret the patterns of protein synthetic activity within *P. aeruginosa* biofilms by IPTG-inducible *gfp* in the PAO1 (pAB1) strain, PAO1 (pMF230) with constitutively expressed mut2 *gfp* was studied as a control (Nivens *et al.*, 2001). As shown in Figure 2.5, fluorescence appeared to be very uniform throughout cell clusters.

The fluorescence did not change in time. The constitutively expressed GFP marker may accumulate and thus reflect the history of the cells rather than the present GFP synthetic activity, which is related to growth physiological state, of *P. aeruginosa* biofilm (Sternberg *et al.*, 1999). Cells with the constitutively expressed GFP can even emit green fluorescence after the cells die.

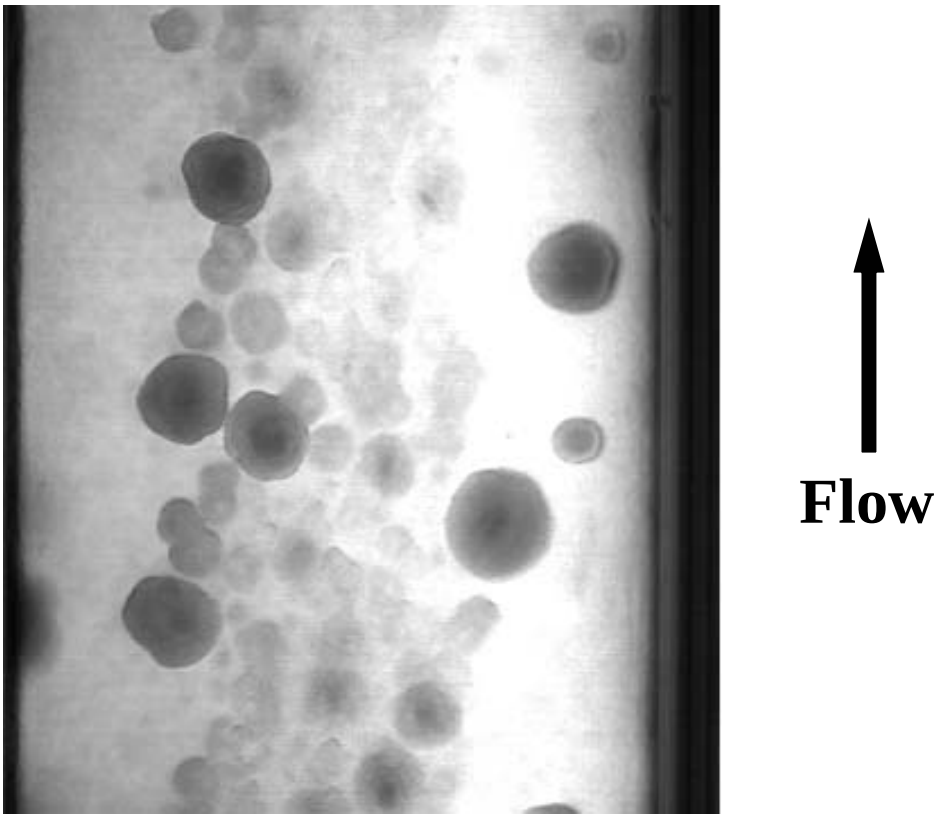

Figure 2.4. Representative transmission image of the *P. aeruginosa* PAO1 (pAB1) biofilm (Imaged by Harrer, A.)

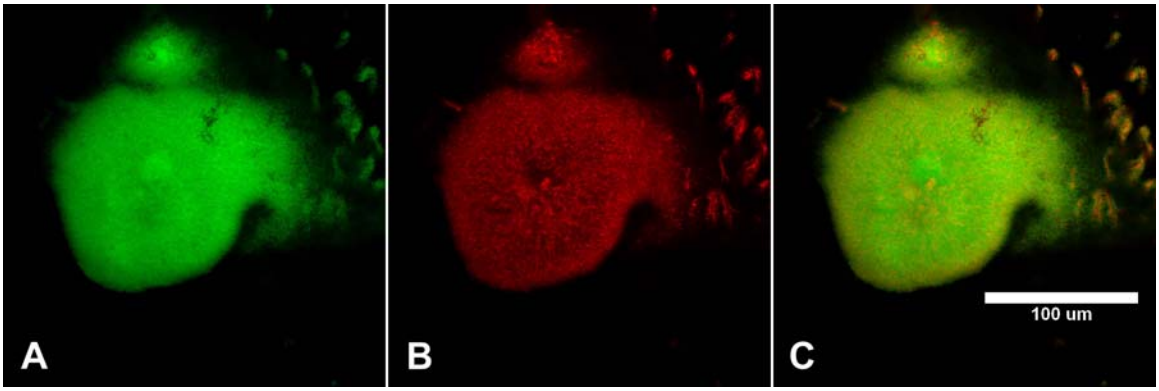

Figure 2.5. Confocal images showing the spatial patterns of constitutively induced GFP expression in the control samples of *P. aeruginosa* PAO1 (pMF230) cell clusters. (A) GFP activity (green); (B) Rhodamine B counterstained biomass distribution (red); (C) Color-combined picture of GFP and rhodamine B stained biomass.

The inducible *gfp* in PAO1 (pAB1) strain, was used to visualize patterns of active growth, protein synthetic activity in particular, within the biofilms.

Time lapse images revealed the transient increase in fluorescence after IPTG addition to the medium (Figure 2.6). Biofilms emitted negligible green fluorescence prior to IPTG induction. At the same spot, with no change in microscope settings, GFP became increasingly intense during the 3 h course of the experiment. Bright green fluorescence was apparent 3 h after adding IPTG to the medium.

Using the Linescan function of MetaMorph, the development of GFP intensities at the center and the edge of individual biofilm clusters over the 3 h induction period was analyzed. The ratio of the green fluorescent intensity at the center of the cluster to the green fluorescent intensity at the edge of the cluster, I_{center}/I_{edge} (where I_{center}: GFP intensity at the center of the cluster; I_{edge}: GFP intensity at the edge of the cluster),

decreased with time. This indicates that GFP expression developed faster at the surface of cell clusters than in the centers. At the end of the 3 h IPTG induction, the ratio I_{center}/I_{edge} was generally less than 1, ranging from 0.13 to 0.95 (Figure 2.7). Image analysis on minute clusters, such as the one with radius of 4 μm, generated bigger experimental errors because fewer data points were available while the pixel number per unit area of images was fixed on a specific image. Furthermore, defining the centers and borders in small clusters was difficult.

After 3 h of IPTG induction, the spatial patterns of GFP expression were studied by scanning single planes of biofilm clusters. These biofilms were counterstained with rhodamine B to reveal the extent of the biomass independent of its activity. With the oxygen activation and 3 h of IPTG induction, greater protein synthetic activity was evident at the surface of most of the clusters than in their centers, which could be visualized directly from single images (Figure 2.8).

Images of single planes within biofilms were quantitatively analyzed using the Linescan function in MetaMorph software as described in the following examples.

By drawing a linear transect (shown as white-bordered boxes in Figure 2.9A) transecting the region of interest, the fluorescence intensity (in this case, GFP) along the line could be described as the corresponding gray level measured by the Linescan function. The intensity could be expressed as either the maximum gray level across the width of the line or the average gray level. In this study, average values were taken. The

setting of line width depends on the size of the cluster. The larger the cluster, the wider the line that was used.

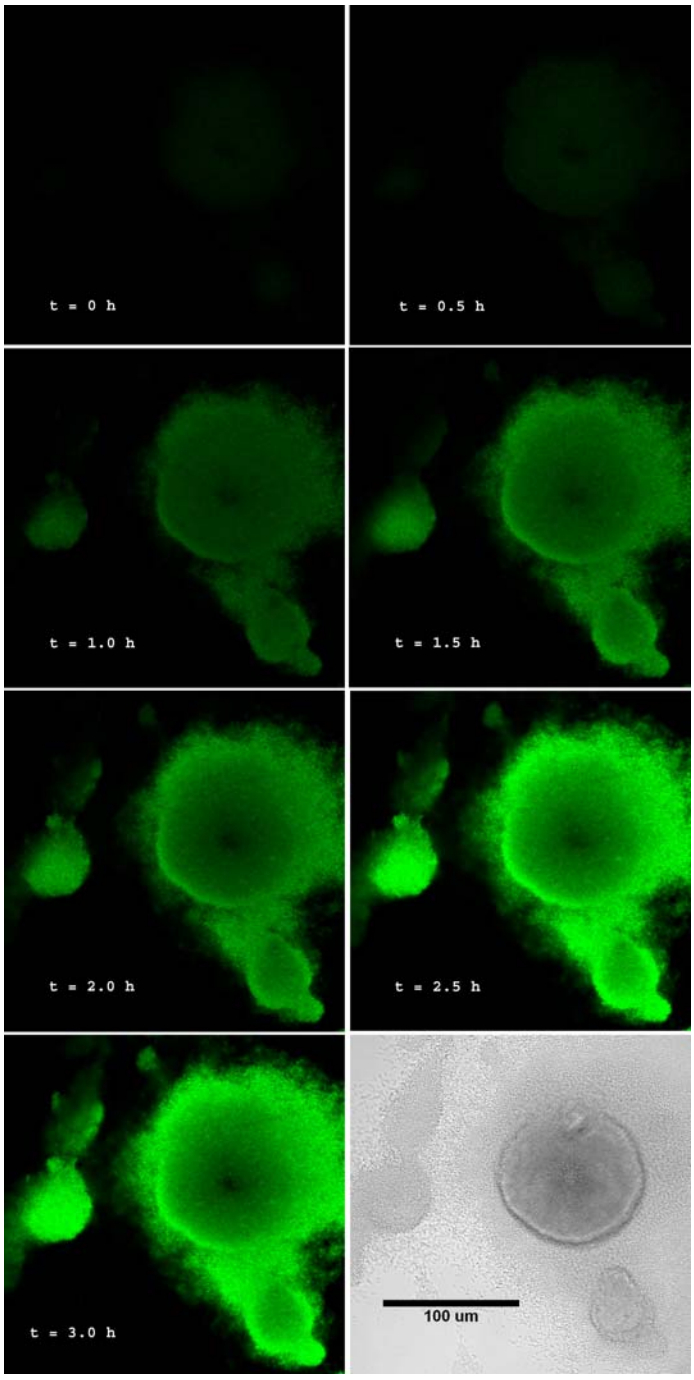

Figure 2.6. Confocal images showing the temporal pattern of GFP expression in a *P. aeruginosa* PAO1 (pAB1) cell cluster during the 3 h of IPTG induction. The last image, which was indicative of the overall biomass distribution, was taken in transmission mode.

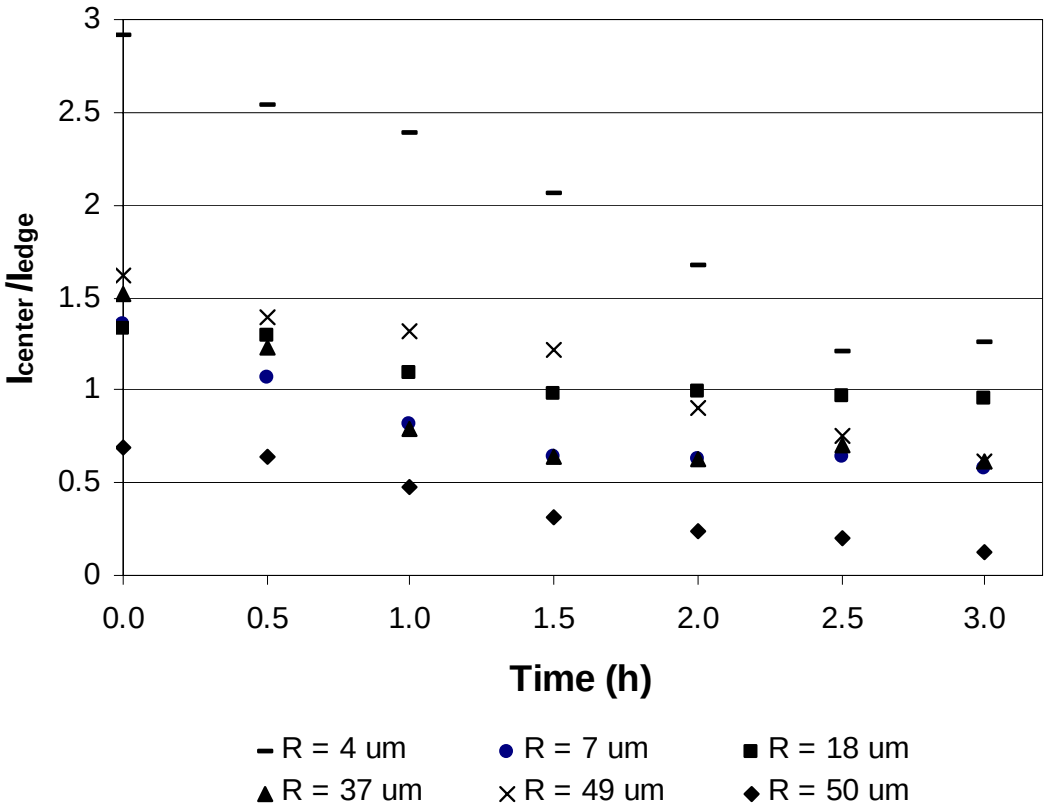

Figure 2.7. In a PAO1 (pAB1) cell cluster, the development of the ratio of the GFP intensity at the center to that of the edge during the 3h of IPTG induction. R: radius of the cluster.

In the single plane image Figure 2.9A, two clusters of different sizes were studied by diametral linescans. The diametral distribution of particular activities (GFP expression by green fluorescence and rhodamine B-stained biomass distribution by red fluorescence) were obtained and are shown in panels B, C.

The linescans for single clusters of different sizes were made to directly illustrate the diametrical GFP expression (Figure 2.11).

In order to obtain the typical value of intensity at a specific radial position, several diametral transects (in this work two perpendicular transects through the cluster center were usually taken to obtain the average value) could be linescanned at the same time. The values of average intensity at the specific radial position, such as I_{center} from the centers of the two transects and I_{edge} from the ends of the two transects, are assumed as typical of the intensity values at the same radial position within the cluster, which simplifies the complicated heterogeneity over the scanned image plane and thus shows the spatial patterns of the GFP expression by the change of variables such as I_{center}/I_{edge} as shown in Figure 2.10.

The GFP of the control sample — PAO1 (pMF230) biofilm appeared to be very uniform. Additionally, one could conclude that GFP synthetic activity is more uniform in smaller clusters and less uniform in larger clusters. Small clusters showed less heterogeneity than the larger ones.

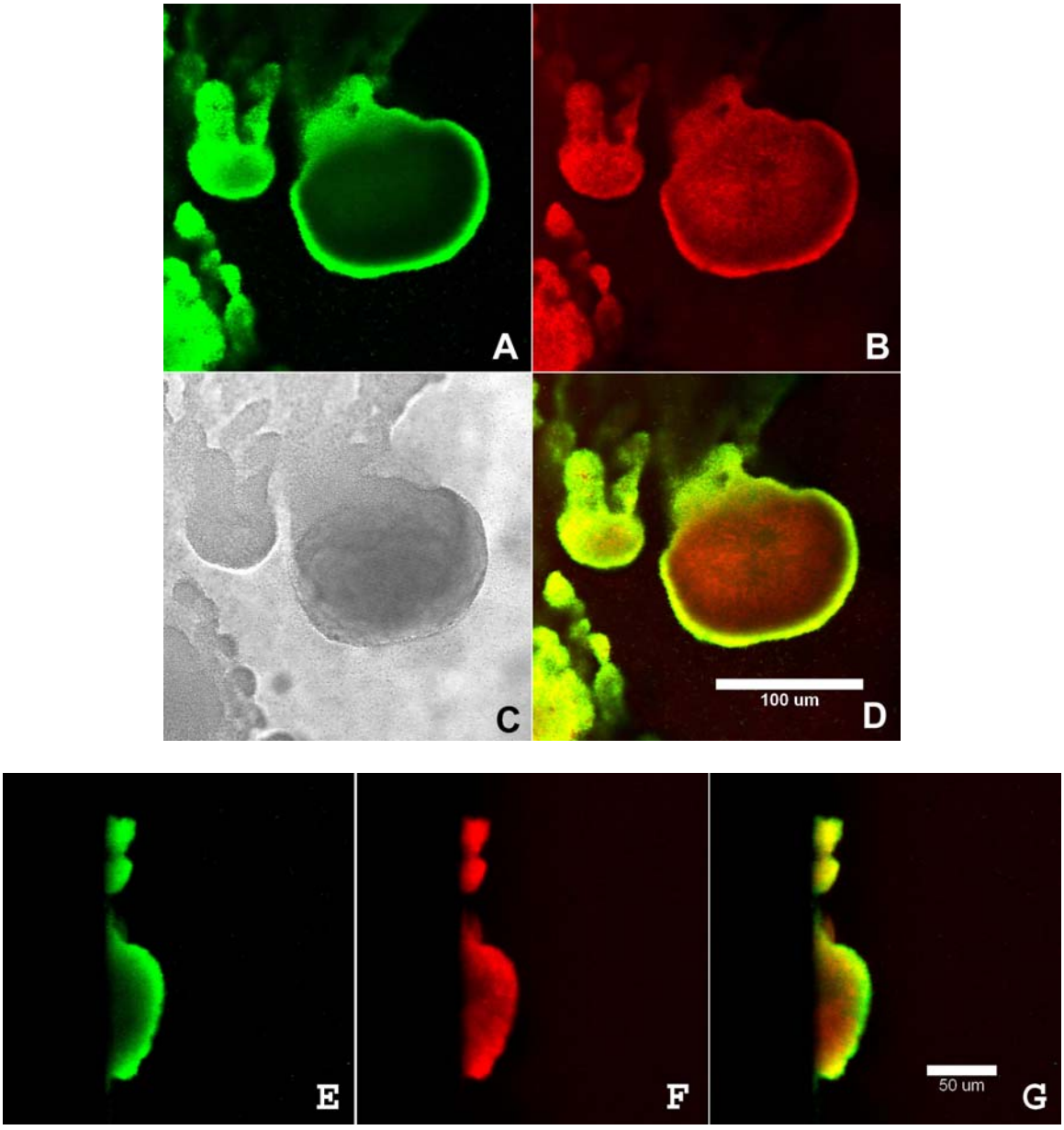

Figure 2.8. Confocal images showing the spatial patterns of GFP expression in *P. aeruginosa* PAO1 (pAB1) cell clusters induced with IPTG for 3 h. View of a cell cluster on the top wall of the flow cell: (A) GFP activity (green); (B) Rhodamine B counterstained biomass distribution (red); (C) Transmission image; (D) Color-combined picture of GFP and rhodamine B counterstained biomass. View of a cell cluster on the side wall of the flow cell: (E) GFP activity (green); (F) Rhodamine B counterstained biomass distribution (red); (G) Color-combined picture of GFP and rhodamine B counterstained biomass.

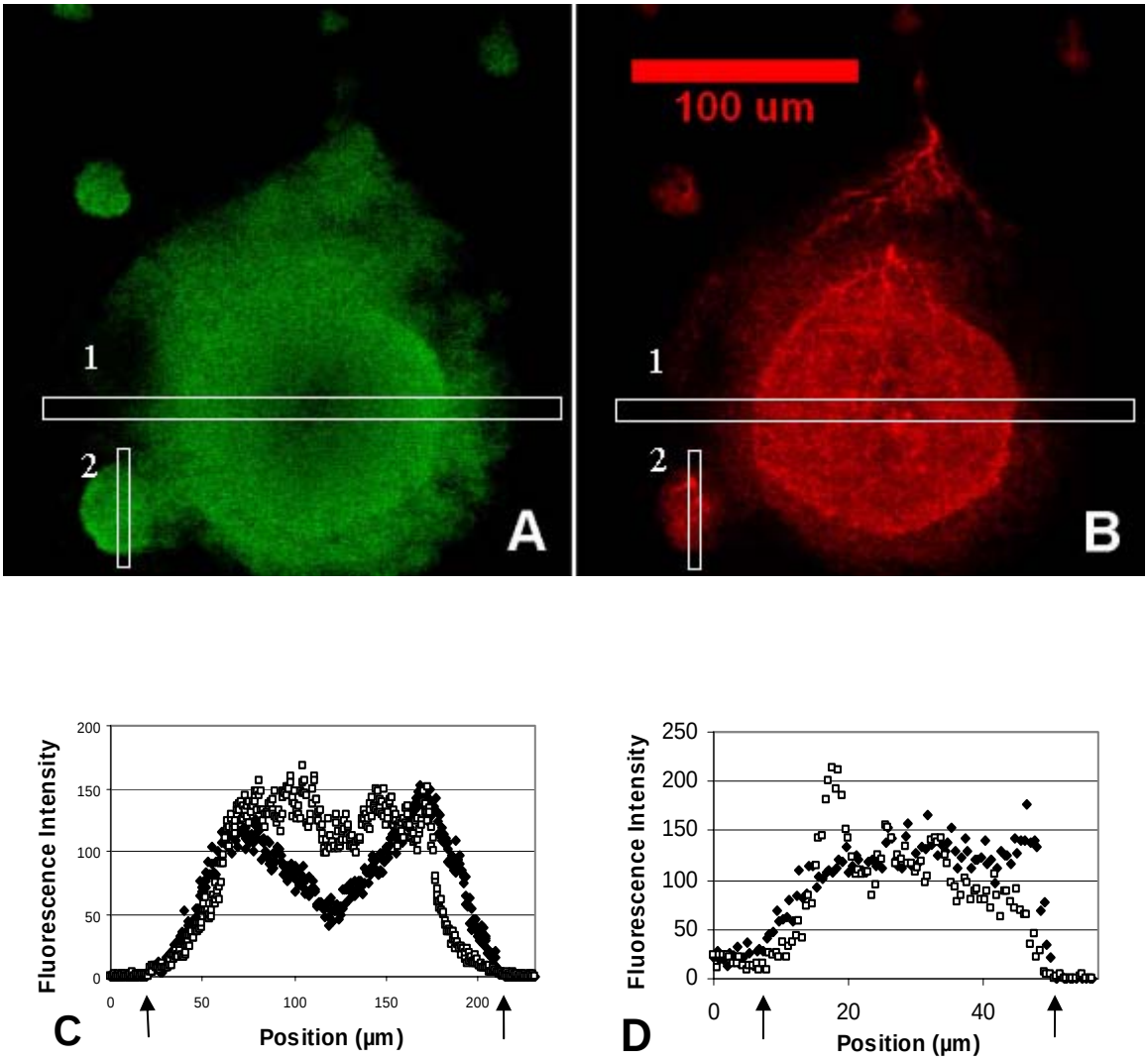

Figure 2.9. Profiles of GFP expression in the induced *P. aeruginosa* PAO1 (pAB1) cell clusters of different sizes obtained by the Linescan analysis. (A) Image of GFP expression showing the location of transects as white boxes; (B) Image of rhodamine B stained biomass showing the same location of transects as shown in (A); (C) Diametral distribution of GFP expression and rhodamine-stained biomass within the white box ($1^{\#}$) over the large cell cluster; (D) Diametral distribution of GFP expression and rhodamine-stained biomass within the white box ($2^{\#}$) over the small cell cluster. ♦ GFP; □ rhodamine B stained biomass. In panels C and D, the two arrows point to the intersections of the diametral transect and the edge of the cluster.

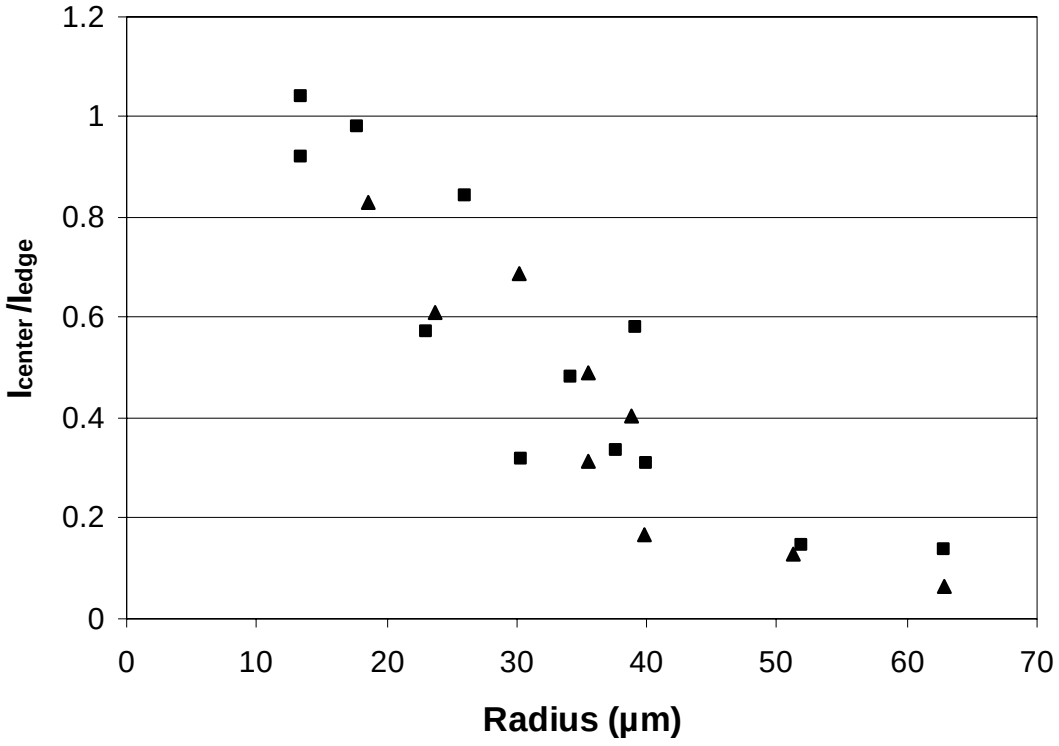

Figure 2.10. The ratio of the GFP intensity at the center to that of the edge along the diametral transects across the induced *P. aeruginosa* PAO1 (pAB1) cell clusters of different sizes. ▲ air points where air was bubbled into the medium flow in the capillary flow cell system; ■ pure oxygen points referring to an experiment in which air bubbles were replaced with pure oxygen bubbles.

R = 10 µm

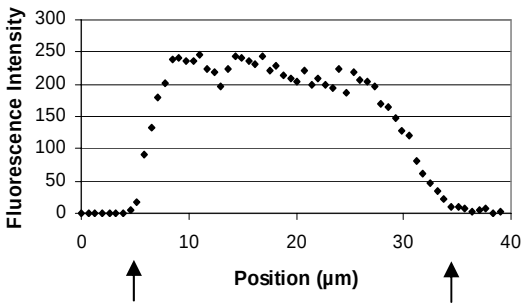

R = 29 µm

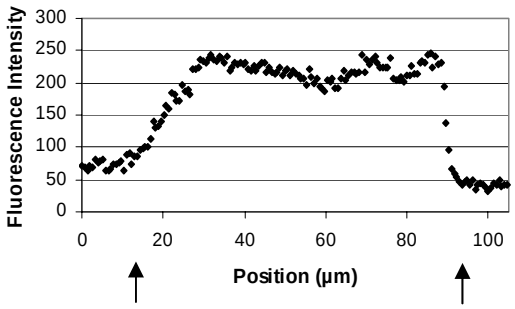

R = 34 µm

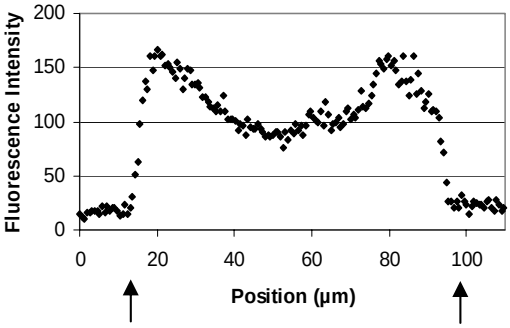

R = 38 µm

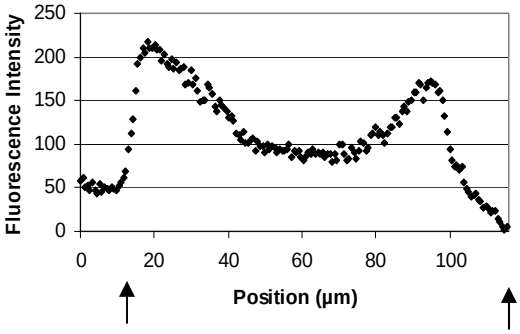

R = 52 µm

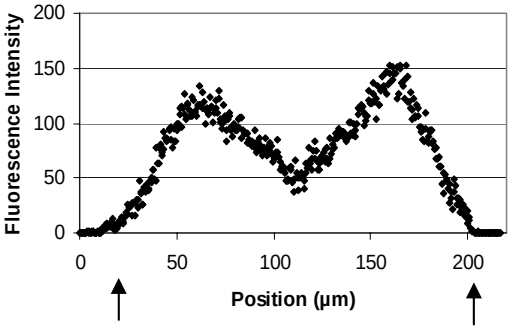

R = 58 µm

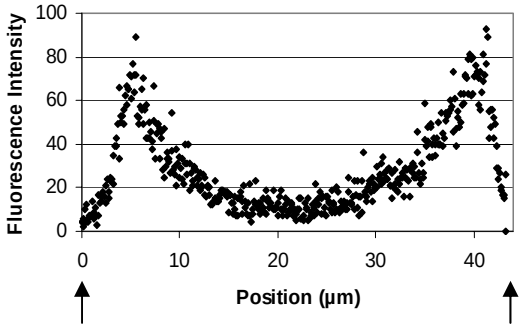

R = 74 µm

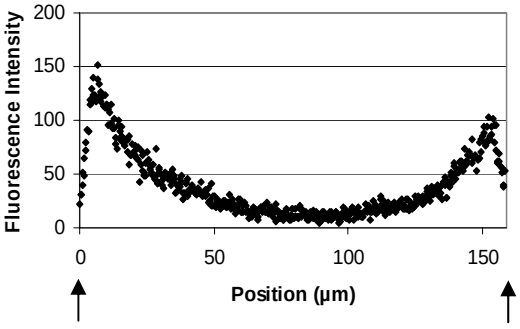

pMF230 (R = 42 µm)

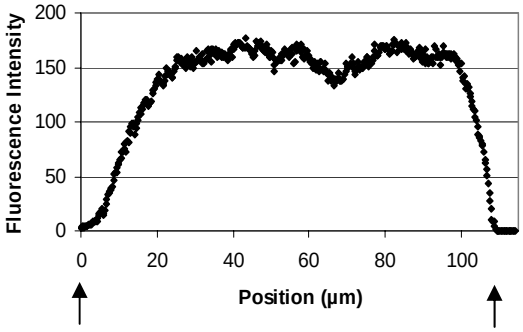

Figure 2.11. GFP expression along the diametral transects of the *P. aeruginosa* PAO1 (pAB1) cell clusters of different sizes. The x-axis is indicative of the diameter axis. The last image is the control sample: constitutively expressed GFP in a PAO1 (pMF230) biofilm cluster. In each panel, the two arrows point to the intersections of the diametral transect and the edge of the cluster.

Discussion

It was realized that individual organisms in biofilm clusters often display heterogeneous behavior with respect to their metabolic activity, growth status, gene expression pattern, etc. (Sternberg *et al.*, 1999). Using fluorescent proteins as a growth rate-related marker has created a revolution in the field of biofilm physiology with respect to visualization of the protein synthetic activity. GFP expression was used to map the spatial growth patterns within *P. aeruginosa* biofilms in this work.

The experiments performed in the present study effectively proved that the patterns of protein synthetic activity in *P. aeruginosa* biofilms could be visualized with the IPTG-inducible *gfp* gene. GFP activity increased during 3 h of IPTG induction and was ready for microscopic observation. It was also clearly indicated that GFP activity developed faster at the surface of cell clusters than in the center. With the air bubble activation and 3 h of IPTG induction, greater GFP synthetic activity was evident at the surface than in the center. GFP activity was less uniform in larger clusters than in small ones. These findings correspond somewhat to those of steady state *P. aeruginosa* biofilms obtained by Sternberg *et al.* using the *gfp* (AAV) physiological probing system. They studied the

spatial patterns on a temporal basis and reported that small colonies consisting of only a few cells were brightly green fluorescent as an indication of relatively high growth rates in the early phases. After approximately 20 h, some colonies became larger. The fluorescence from the central parts of these colonies was reduced, probably due to a lowered rate of GFP synthesis. At the surface of the colonies, most cells were still fluorescent, indicating locally higher activity closer to the void space. The smaller microcolonies, however, were still fluorescent throughout and remained so for some time. Similarly, Wentland *et al.* used acridine orange to visualize the spatial variations in growth rate within *K. pneumoniae* biofilms and revealed a zone of rapid growth running near the biofilm-bulk fluid interface and a zone of slow growth in the biofilm interior (Wentland *et al.*, 1996).

The oxygen distribution within biofilms was strongly correlated with the complex structures consisting of microbial cell clusters (discrete aggregates of densely packed cells) and interstitial voids (de Beer *et al.*, 1994). The stratified patterns of protein synthesis are probably a reflection of oxygen limitation in these biofilms. In the Keck project medium that was used in this work, no electron acceptor other than oxygen was present. *P. aeruginosa* is unable to grow in the absence of oxygen in this medium. Oxygen is known to be commonly limiting in biofilms formed by aerobic bacteria, including *Pseudomonads*. Cells at the surfaces of large cell clusters, or at any point in small cell clusters, have access to oxygen coming from the bulk fluid and exhibit protein synthesis in response to a stimulus. Cells in the interior of larger cell clusters find

themselves in anoxic zones and are incapable of much metabolic activity. Additionally, molecular oxygen is involved with the formation the final fluorophore independent of enzymes or cofactors. Even if the GFP is actively synthesized in the presence of oxygen, it might fail to fluoresce due to the limited oxygen concentration for chromophore generation.

CHAPTER 3

SPATIAL GROWTH PATTERNS OF *PSEUDOMONAS AERUGINOSA* DRIP-FLOW REACTOR BIOFILMS VISUALIZED BY USING AN INDUCIBLE GREEN FLUORESCENT PROTEIN

Introduction

Biofilms of *P. aeruginosa* PAO1 (pAB1) grow much more slowly compared to the wide-type PAO1 biofilms because of the high energy consumption requirement by the plasmids. Moreover, due to the relatively high shear inside the capillary, even the mature capillary reactors are very thin and not evidently visible, which makes it hard to study the spatial heterogeneity and growth patterns within the biofilm clusters because few big clusters were available. In contrast, the drip-flow reactor designed by the Center for Biofilm Engineering has very low shear caused by the slow gravity flow conditions. The biofilms grown in this reactor detach less and thus are thicker than those grown in other reactors with higher shear force, such as capillary reactors. Mature drip-flow reactor biofilms are loosely attached to the growth surface, whereas the capillary reactor biofilms are more tightly fixed with a larger relative detachment rate.

The drip-flow reactor system has some disadvantages for microscopic examination of the biofilms compared to the capillary reactor. The latter allows nondestructive, in situ observation of living, fully hydrated biofilms without the need for harsh chemical fixation or embedding techniques (Wilson T., 1990), which favors the study on a temporal basis for the patterns of GFP expression within these capillary reactors during IPTG induction. However, the resolution limits of optical microscopy impede the direct examination through the thick drip-flow reactors. A method for rapid and minimally disruptive embedding and sectioning of thick biofilms has thus been developed. Biofilms were cryoembedded using a commercial tissue embedding medium. Quick freezing using dry ice minimized ice crystal formation in the specimen and allowed the embedded biofilm to be separated easily from the substratum. Microscopic examination of the substratum surface after biofilm removal indicated that less than a monolayer of attached cells remained. Frozen sections, 5-µm-thick, were cut with a cryostat and examined by light microscopy. The cryoembedding technique preserved biofilm structural features including an irregular surface, water channels, local protrusions up to 500 µm thick, and a well-defined substratum interface. (Yu *et al.*, 1994). The biofilms stopped growing upon sampling and embedding.

Since the thickness (Z dimension) of the cross section, 5 µm, is negligible compared to the X-Y dimension, the three-dimensional structure of the drip-flow reactors can not be rebuilt. The Z-position image stacks of capillary reactors, however, can be used to visualize the reconstructed three-dimensional structure.

The chapter describes how drip-flow reactor system was employed to grow *P. aeruginosa* biofilms as a complementary tool to the capillary reactor system, in order to obtain thicker biofilms and further study the spatial patterns of GFP synthetic activity.

Materials and Methods

Strains, Plasmids and Media

P. aeruginosa PAO1 (pAB1) strain was used in this section. The strain was grown in the Keck project medium (Table 1.1). Medium was prepared as described in Chapter 2. GFP synthetic activity within these biofilms has been introduced in Chapter 2.

Drip-Flow Reactor System

Biofilms were cultivated in a drip-flow reactor with individual channel dimensions of 98.0 mm by 18.4 mm by 12.3 mm under gravity flow conditions. The reactor was made up of four parallel channels in a polysulfone base with transparent lids, air vents, rubber septum for inoculation and medium entry, all connected by effluent tubing from the bottom of the base (Figure 3.1). Biofilms were grown on the stainless steel coupons inserted into each channel. During bacterial cultivation, the reactor was resting on 10º

tilted support platform. Keck project medium was dripped onto the metal coupons at a rate of 1 ml/min and flowed down the coupons in a gravity flow manner. Due to the slow medium dripping and gravity flow over the coupon surface, the drip-flow reactor has a very low fluid shear, which decreases the biofilm detachment greatly. Biofilms grown in the drip-flow reactor are thus much thicker than those grown in other reactors with higher shear.

Cultivation Procedure

PAO1 (pAB1) biofilms were grown on coupon surfaces for 5 d with Keck project medium dripping at ambient temperature (23^{o}C). The medium, reactor, and the remaining system components were autoclaved separately. Working in a laminar flow hood after allowing hot items to cool, the drip-flow reactor was connected to the effluent tubing and waste carboy. They were removed to the laboratory bench. For inoculation, the effluent tubing was clamped immediately downstream of the reactor. After sterilizing the rubber septa above the reactor channels, about 15 ml of Keck project medium was added into each channel by a syringe, and about 1 ml of an overnight culture of the PAO1 (pAB1) strain (optical density at 600 nm of 0.001 to 0.005) inoculated to each channel. The system was placed on a level bench for 18 h for attachment of bacteria to the coupon surface. Meanwhile, the autoclaved inflow part of the system, including the medium feed carboy and inflow tubing with sterile needles, was plumbed in the laminar flow hood

prior to initiating the medium flow. After 18 h, the clamps were removed from the effluent tubing and medium drip flow was initiated at a flow rate of 1 ml/min. Then the reactor was placed on a 10º tilted support platform to create a slow gravity flow environment for biofilm growth.

Sampling and Preprocessing

After 5 d of growth, the four mature biofilm samples on the coupons were treated separately by IPTG or rhodamine B counterstaining (Table 3.1).

Table 3.1. Pretreatment of the drip-flow reactor biofilms prior to microscopic examination of GFP expression

	Sample	Control Sample	IPTG Control Sample	Counterstained Control Sample
IPTG induction	3 h	——	3 h	——
rhodamine B counterstaining	10 min	——	——	10 min

The sample and the IPTG control sample were induced by IPTG for 3 h before the coupons were withdrawn from the channels. A staining container with separate chambers fitting the coupons was used for staining. The sample and counterstained control sample were placed in the staining container with the biofilm side up and then submerged in 5 ml

of 50 mg/ml rhodamine B solution. The liquid was removed from the staining container after 10 min. Then all the samples were ready for cryoembedding.

Cryoembedding

Tissue-TEK O.C.T. Compound, Sakura Finitek #4583, was used to embed the biofilm samples and provide a matrix for frozen sectioning. The compound was available through VWR Scientific Products, Inc. A small, dime-sized amount of embedding medium was dispensed onto the coupon with the biofilm side up. Then the coupon was immediately placed on dry ice and the embedding medium allowed to rapidly freeze. The frozen colony biofilm embedded in O.C.T. was separated from the coupons by gently bending the coupons and then turned over to embed the side that was previously attached to the substratum. The second step of cryoembedding created a layered matrix in which biofilm was completely surrounded by O.C.T. The colony biofilm specimen was then wrapped in aluminum foil and stored at -70°C or directly brought to cryostat for cryosectioning.

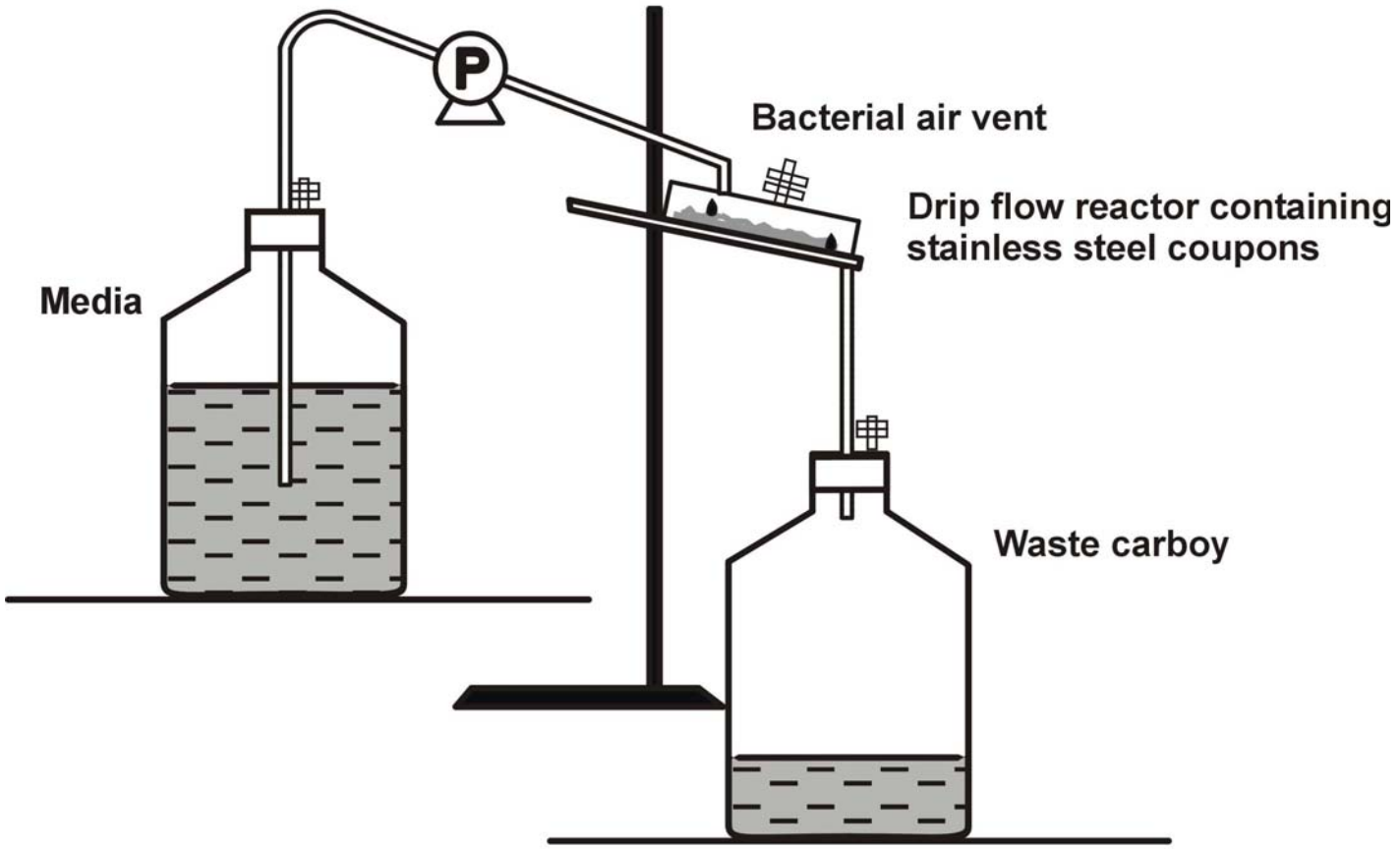

Figure 3.1. Schematic of drip-flow reactor system used to grow *P. aeruginosa* PAO1 (pAB1) biofilms

Cryostat Sectioning

Frozen colony biofilms were cut into 5-µm-thick sections with a Leica CM 1850 cryostat machine operated at –20°C. The colony biofilm to be cryosectioned was cut into halves. One half of the frozen colony was attached to the metal chuck with a dime-sized amount of embedding medium so that the horizontal part of the colony (the part where the bacteria were exposed) was parallel to the flat surface of the chuck. After allowing the embedding medium to freeze, the frozen colony half was securely mounted on a precooled (–20°C) chuck. The chuck was then secured into its place close to the blade of the cryostat. The frozen colony was aligned perpendicular to the microtome blade. The section thickness was set at 5 µm. A flat 5-µm-thick slice of biofilm was cut off and slowly pulled onto the stage using a paintbrush. Each cross-section was mounted on a positive-charged Superfrost Plus glass slide (Fisher Scientific, Pittsburgh, PA) for microscopic examination.

Microscopic Examination

The cross sections were examined using a Nikon Eclipse E800 epifluorescece microscope. According to the excitation and emission spectra of GFP (Figure 2.1) and rhodamine B (Chapter 2), a fluorescein isothiocyanate (FITC) filter set containing an exciter (wavelength of 465-495 nm), a dichroic mirror (model DM-505), and an emitter

(wavelength of 515-555 nm) was set for GFP fluorescence (green). A tetramethylrhodamine isothiocyanate (TRITC) filter set containing an exciter (wavelength of 540 nm), a dichroic mirror (model DM-565), and an emitter (wavelength of 630 nm) was set for rhodamine B fluorescence (red). A 10× dry lens was used.

Image Analysis by MetaMorph Software

Quantitative image analysis was performed using the built-in Linescan function in MetaMorph image analysis software as described in Chapter 2.

Results

In the present study, thick *P. aeruginosa* biofilms were obtained using the low-shear drip-flow reactor system. The individual measurements of biofilm thickness ranged from approximately 64 to approximately 220 μm with a mean value of 145.5 ± 47.6 μm.

To confirm the IPTG-inducible GFP expression in the *P. aeruginosa* biofilms, three kinds of controls were obtained as shown in Table 3.1. It was manifest that IPTG induction was required for GFP expression since the control sample without IPTG induction was totally dark (Figure 3.2).

After 3 h of IPTG induction, sectioned biofilm samples were observed and single scanning pictures collected (for example, Figure 3.3A-D). There is some blurring of the image, presumably due to overlapping bacterial cells in the 5-μm-thick section (Yu *et al.*, 1994). Quantitative analysis was performed by using the Linescan function to study the spatial patterns of GFP expression within *P. aeruginosa* biofilms. To do linescanning, the length of the sectioned biofilms was assumed to be in X direction, the thickness of the section in Z direction. Lines were located in Z direction at different spots, perpendicular to the sectioned biofilms. Average value across the line width (X direction) represented the intensity at the specific depth (Z position) (Figure 3.3D). Thus, the GFP intensity and biomass distribution along the biofilm depth could be obtained (Figure 3.3E).

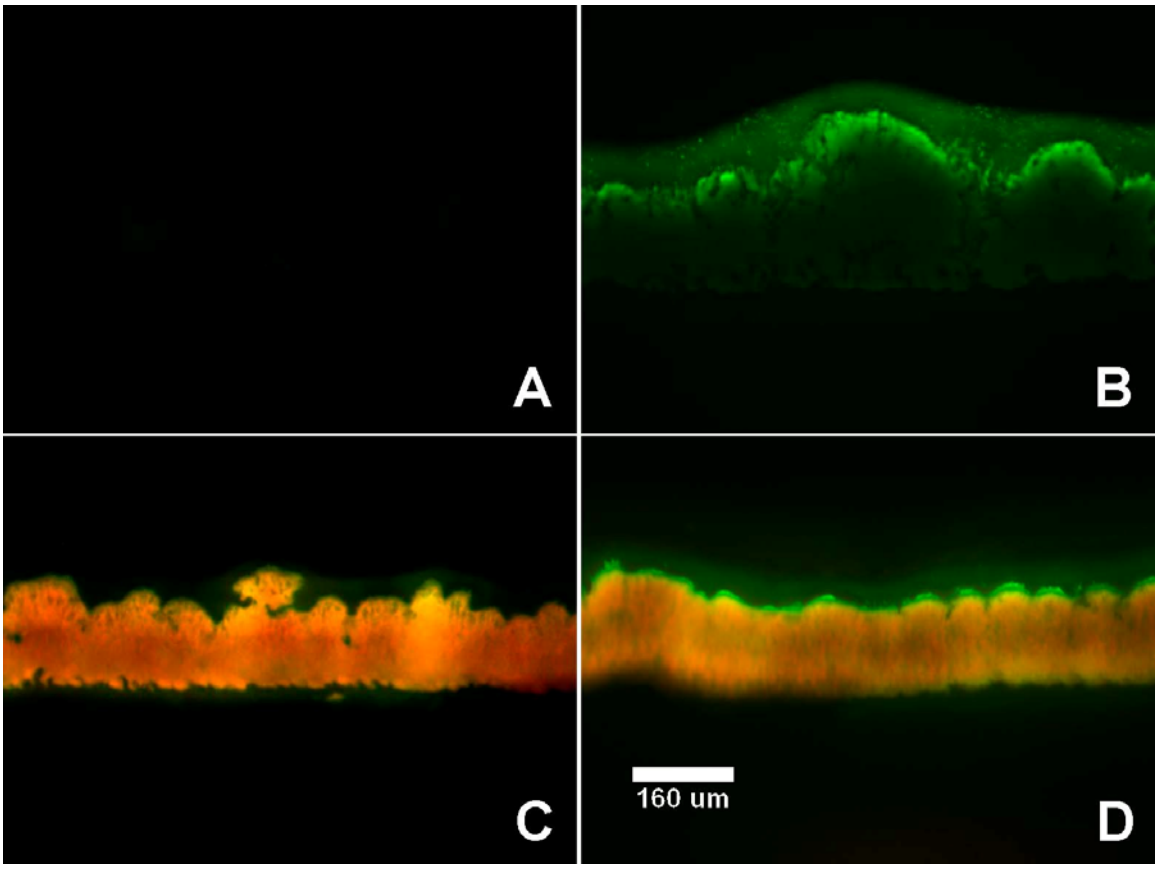

Figure 3.2. Nikon light microscopic images showing the spatial patterns of GFP expression in the control samples and the sample of *P. aeruginosa* PAO1 (pAB1) biofilm cross sections: (A) Control sample without IPTG induction and rhodamine B counterstaining; (B) IPTG control sample with 3 h of IPTG induction but without rhodamine B counterstaining; (C) Rhodamine B counterstaining control sample with rhodamine B counterstaining but without IPTG induction; (D) Sample showing the spatial patterns of GFP expression (green) in sectioned *P. aeruginosa* PAO1 (pAB1) biofilms induced with IPTG for 3 h and counterstained by rhodamine B (red). The images are oriented with the substrata at the bottom of the pictures.

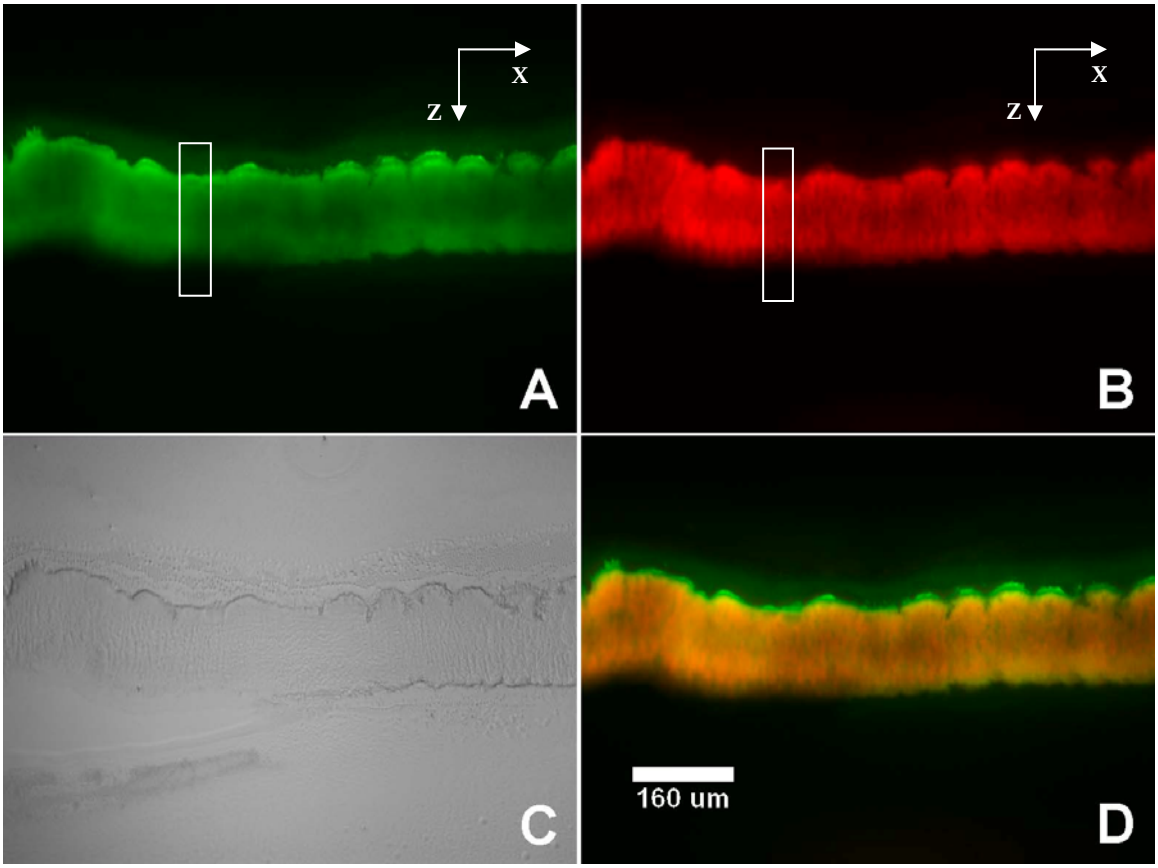
x
z
A
x
z
B
C
160 um
D

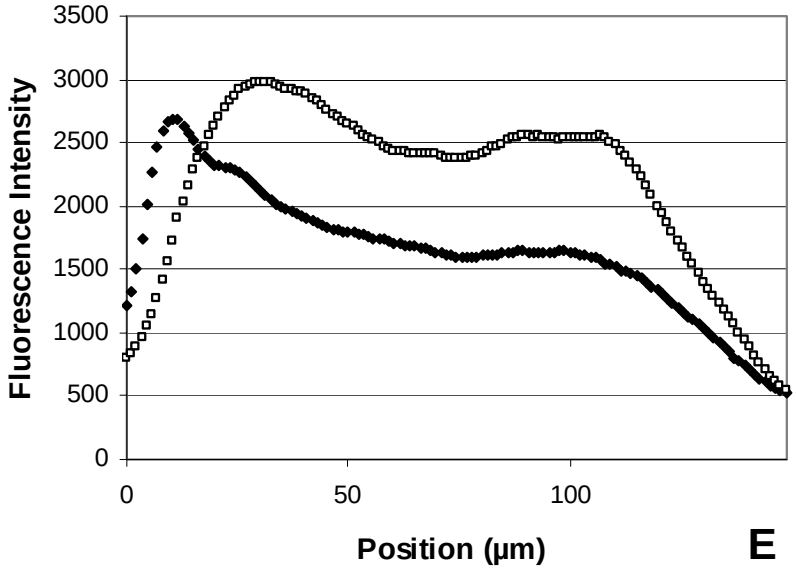
Fluorescence Intensity
3500
3000
2500
2000
1500
1000
500
0
0
50
100
Position (µm)
E

Figure 3.3. Nikon light microscopic images showing the spatial patterns of GFP expression in *P. aeruginosa* PAO1 (pAB1) biofilm cross sections induced with IPTG for 3 h and the schematic of quantitative analysis at representative location using the Linescan function. (A) GFP activity (green); (B) Rhodamine B counterstained biomass distribution (red). Rhodamine B stained area represents the total biomass. (C) Transmitted-light image; (D) Color-combined picture of GFP and rhodamine B stained biomass. The Linescan transect was located as white boxes. (E) GFP expression and rhodamine B counterstained biomass distribution within the white box along the biofilm depth. The origin of the "Position" axis represents the biofilm-bulk fluid interface. The end of the "Position" axis represents the substratum. ♦, GFP; □ rhodamine B stained biomass. The images are oriented with the substrata at the bottom of the pictures. The position axis was directed from the biofilm-bulk fluid interface side to the substratum (Z direction). The position of zero represents the biofilm-bulk fluid interface.

The linescans for single biofilm cross sections were made to directly show the depth-dependent GFP expression (Figure 3.4). Each GFP expression graph has a peak near the biofilm-bulk fluid interface and a relatively flat shoulder close to the substratum. The GFP active area was assumed to occur within the peak span. The thicker the biofilm was, the sharper the peak and the flatter and longer the shoulder. Thicker biofilms had a lower percentage of GFP activity area.

The direct illustration in Figure 3.4 was quantified to model the GFP activity. The thickness of GFP active area (L_{GFP}) and the ratio of GFP activity thickness to the biofilm thickness (L_{GFP} /$L_{biofilm}$) were graphed separately versus biofilm thicknesses.

Figure 3.5 shows that the thickness of GFP activity area, does not depend on the biofilm thickness. Individual measurements of L_{GFP} ranged from approximately 46 to approximately 79 μm with a mean value of 58.8 ± 8.1 μm. In *P. aeruginosa* PAO1

(pAB1) biofilms, GFP activity was almost concentrated on the top 60 μm of the biofilm where oxygen and nutrients enter the biofilm matrix from the medium.

$L_{GFP}/L_{biofilm}$ decreased as biofilms got thicker (Figure 3.6), which is consistent with the patterns viewed directly in Figure 3.4 and Figure 3.5. In 5-d *P. aeruginosa* PAO1 (pAB1) biofilms, the ratio $L_{GFP}/L_{biofilm}$ was generally less than 1, ranging from 0.28 to 1.05. The value above 1.0 may be generated by the fluorescence blurring at the edge of biofilm sections.

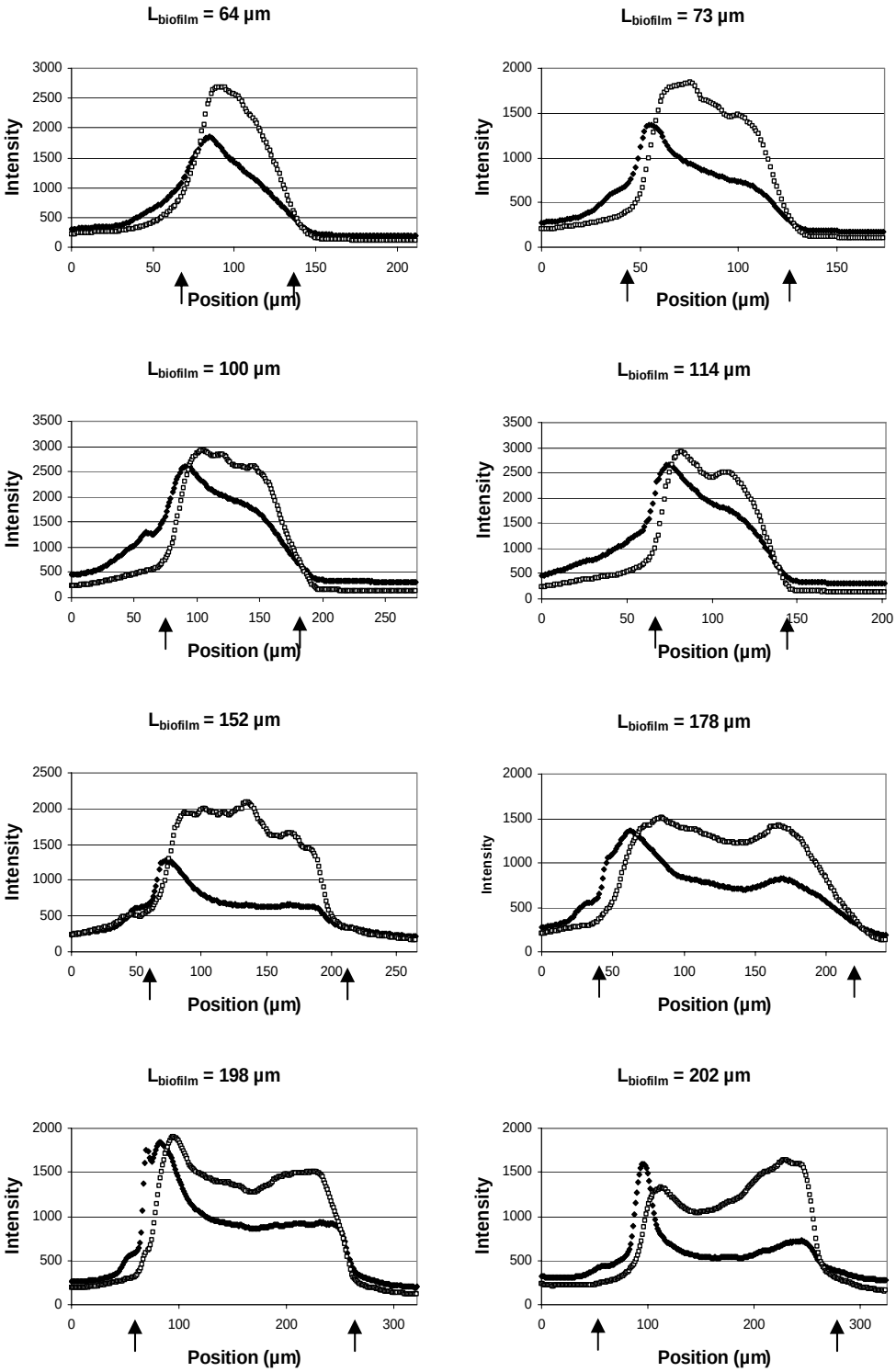
$L_{biofilm}$ = 64 µm
Intensity
Position (µm)
$L_{biofilm}$ = 73 µm
Intensity
Position (µm)
$L_{biofilm}$ = 100 µm
Intensity
Position (µm)
$L_{biofilm}$ = 114 µm
Intensity
Position (µm)
$L_{biofilm}$ = 152 µm
Intensity
Position (µm)
$L_{biofilm}$ = 178 µm
Intensity
Position (µm)
$L_{biofilm}$ = 198 µm
Intensity
Position (µm)
$L_{biofilm}$ = 202 µm
Intensity
Position (µm)

Figure 3.4. Profiles of GFP expression along the linear transects across the sectioned *P. aeruginosa* PAO1 (pAB1) biofilms of different thicknesses obtained by the Linescan analysis. The position axis represents the line in the Z dimension shown in Figure 3.3E. In each panel, the first arrow points to the biofilm-bulk fluid interface, the second one to the substratum. ♦, GFP; □, rhodamine B stained biomass. $L_{biofilm}$: total biofilm thickness as determined from rhodamine B counterstained biomass.

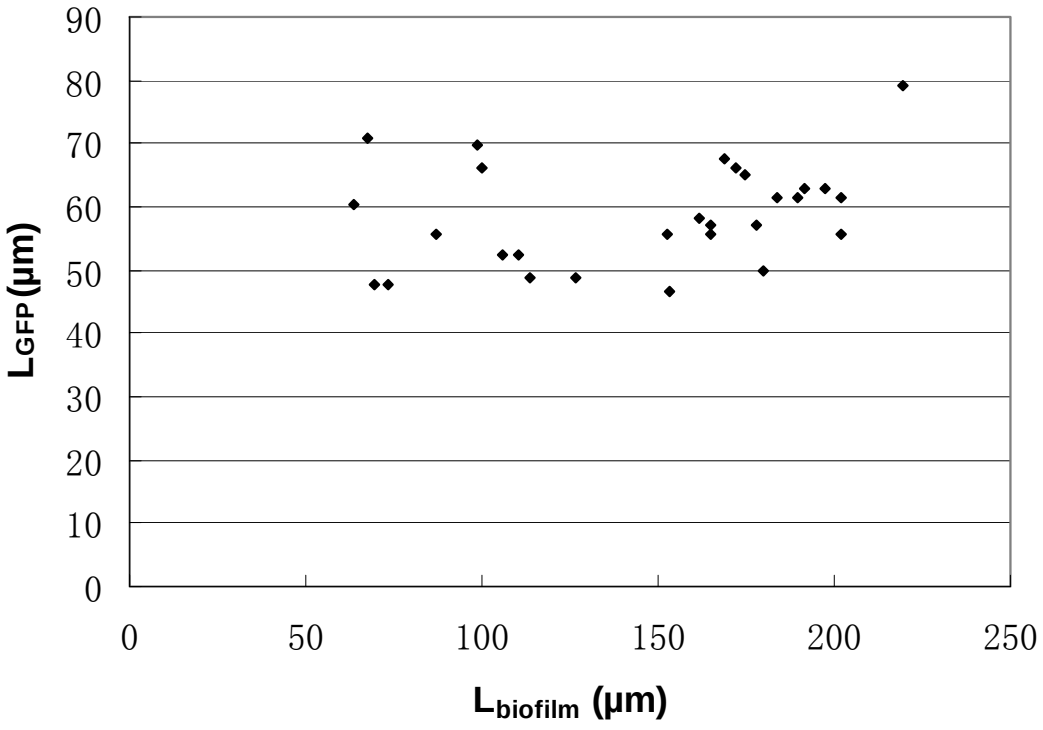

Figure 3.5. The dimension of GFP expression zone in different-depth biofilm cross sections. L_{GFP}: dimension of the zone of GFP expression, indicated by the span of the GFP activity peak close to the biofilm-bulk fluid interface (examples as shown in Figure 3.3E and Figure 3.4); $L_{biofilm}$: total biofilm thickness.

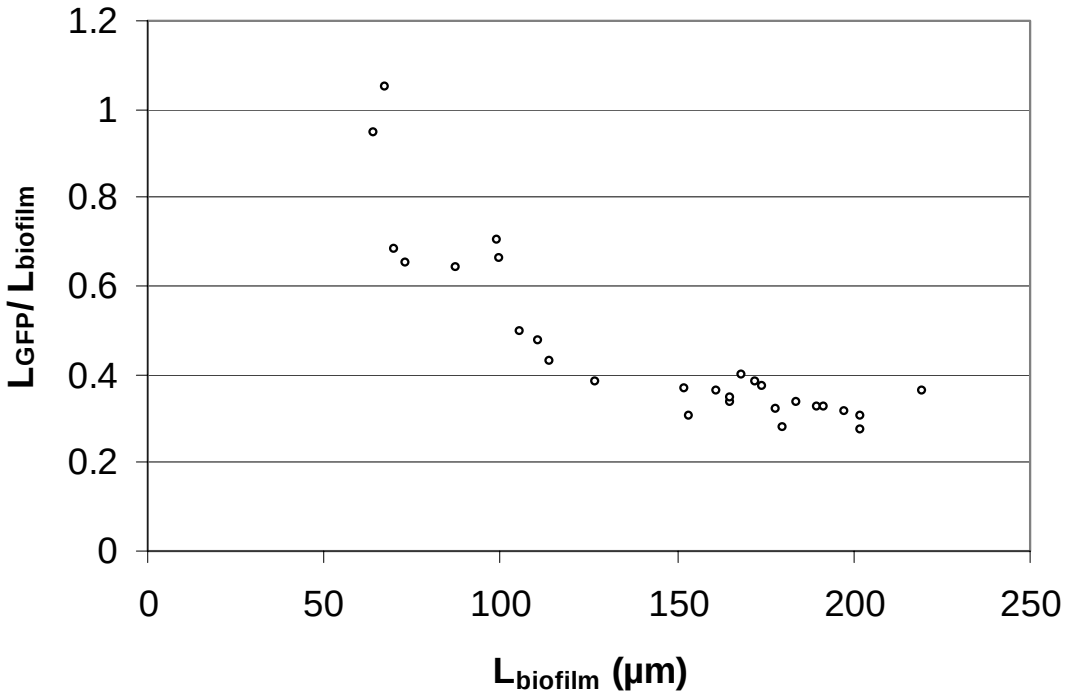

Figure 3.6. The ratio of thickness of GFP expression zone to the total biofilm thickness with respect to different-depth biofilm cross sections.

Discussion

Previous research (Chapter 2) has shown that PAO1 strain carrying the pAB1 plasmid can be used to map spatial patterns of protein synthetic activity in *P. aeruginosa* biofilms. Biofilms as thick as approximately 10 to 74 µm grown in the capillary reactor had been studied in situ. Much thicker biofilms, ranging from approximately 64 to

approximately 220 μm with a mean value of 145.5 ± 47.6 μm, were sampled using the drip-flow reactor system in the present study.

The structures of the capillary reactor biofilm looked different from the drip-flow reactor biofilm. The former consisted of biofilm clusters and void spaces like water channels; the latter was almost a slab biofilm with a few clusters sticking out and void spaces. However, the penetration and distribution of oxygen and nutrients within these biofilms could be interrelated: the edge of the capillary reactor corresponded to the level biofilm-bulk fluid interface of drip-flow reactor with easy access to oxygen and nutrients; the center of the capillary reactor was the counterpart of the biofilm-substratum interface of drip-flow reactor biofilm, the place requiring oxygen and nutrients to travel the farthest. Consequently, the study of thicker sectioned biofilms showed a similar heterogeneous structure of the biofilms: greater GFP expression in the area close to the biofilm-bulk fluid interface than in regions close to the biofilm-substratum interface. Both of these may be related to oxygen-limitation as described in Chapter 2.

CHAPTER 4

SPATIAL GROWTH PATTERNS OF *PSEUDOMONAS AERUGINOSA* DRIP-FLOW REACTOR BIOFILMS VISUALIZED BY INDUCTION OF ALKALINE PHOSPHATASE

Introduction

In a thick aging biofilm the deep-internal portions of biofilms are hypothesized to experience starvation and slow growth due to nutrient limitation (Xu *et al.*, 1999). As introduced in Chapter 1, starvation is an important physiological factor for reduced biofilm susceptibility. Bacteria isolated on low-nutrient media from the environment are physiologically more tolerant than those isolated on rich media (Harowitz *et al.*, 1983).

Microbial physiological changes induced by phosphate starvation have long been studied. Inorganic polyphosphate is needed for swimming, swarming, and twitching motilities of *P. aeruginosa* (Rashid and Kornberg, 2000), and flagellar and twitching motility are necessary for *P. aeruginosa* biofilm development (O'Toole and Kolter, 1998). Hou *et al.* (1966) suggested that ribosomal material would appear to be a logical substrate capable of satisfying both the maintenance energy requirements of the cell and the need

for metabolites, such as phosphate, when it is considered that the cessation of growth removes the requirement for a large complement of protein-synthesizing ribosomes.

Mallette *et al.* examined the growth and survival of planktonic *E. coli* cultures in phosphate-limiting medium and were unable to detect a threshold requirement for phosphate analogous to the "energy of maintenance" requirement found for glucose (Mallette *et al.*, 1964). Under phosphate limitation conditions, alkaline phosphatase (APase) accounts for about 6% of the total protein synthesized by the cell. APase was first discovered by Hou *et al.* (1966). The changes occurring in planktonic *P. aeruginosa* cultures were reported. After 24 h period of starvation, specific activity of alkaline phosphomonoesterase increased several hundred fold during a 24-h period of phosphate starvation of planktonic cultures of the *P. aeruginosa*. Additionally, a threshold requirement for phosphate analogous to the "energy of maintenance" was not detected (Hou *et al.*, 1966). Thus, phosphate salts in the regular Keck project medium were completely omitted to create a non-phosphate environment during phosphate starvation in this study. APase expression in response to phosphate starvation was shown to be spatially and temporally heterogeneous in bacterial biofilms and colonies (Huang *et al.*, 1998; Xu *et al.*, 1998). The purpose of the work in this chapter was to test the APase synthetic activity induced by phosphate starvation and map the heterogeneous spatial patterns of the APase expression within *P. aeruginosa* biofilms.

Materials and Methods

Strains, Plasmids and Media

P. aeruginosa PAO1 (pAB1) strain was grown in regular Keck project medium, named high-P_i medium in this chapter (Table 1.1), for 104 h, and then transferred to a P_i-deficient medium environment for 16 h of growth during phosphate starvation. The high-P_i medium was prepared as introduced in Chapter 2. The P_i-deficient medium was made by replacing the phosphate salts of the regular Keck project medium (in this case sodium phosphate monobasic, potassium phosphate dibasic) with morpholinopropanesulfonic acid (MOPS) at the same molar concentration, 4.9 mM (Table 4.1).

Table 4.1. P_i-deficient Keck project medium for *P. aeruginosa* growth during phosphate starvation

Ingredient	Formula	Concentration (g/L)
Glutamic Acid (sodium salt)	$C_5H_8NO_4Na$	0.1522 g
Glycerol	$C_3O_3H_8$	0.4605 g
Magnesium Sulfate	$MgSO_4$-$7H_20$	0.0493 g
MOPS	MOPS	1.0256 g
Sodium Chloride	NaCl	8.4738 g

pH value adjusted to 7.

Cultivation Procedure

PAO1 (pAB1) biofilms were cultivated using the drip-flow reactor system as introduced in Chapter 3. The biofilms were grown on stainless steel coupon surfaces with high-P_i Keck project medium for 104 h and then with P_i-deficient Keck project medium for 16 h at ambient temperature (23^oC). The drip-flow reactor system was used to grow the thick biofilms. The preparation of the medium, assembly of the drip-flow reactor system, inoculation and medium flow initiation were operated the same as described in Chapter 3. After 104 h of cultivation, one channel was continuously fed with high-P_i medium to obtain the high-P_i control sample. The other three channels were switched to P_i-deficient medium feeding by changing the medium feed carboy in a laminar flow hood.

Sampling and Preprocessing

ELF (enzyme-labeled fluorescence) 97 is a water-soluble APase substrate. This substrate fluoresces only weakly in the blue range; however, once its phosphate is enzymatically removed, an intensely fluorescent yellow-green precipitate appears at the site of enzymatic activity. Since the emission spectra of the ELF 97 precipitate and the original blue fluorescent labels are distinct, the signal emitted by cells expressing APase and the signal emitted by cells not expressing APase can be simultaneously visualized by yellow-green and blue fluorescence, respectively. This process is termed as enzyme-labeled fluorescence (ELF) (Molecular Probes, Inc., 2001).

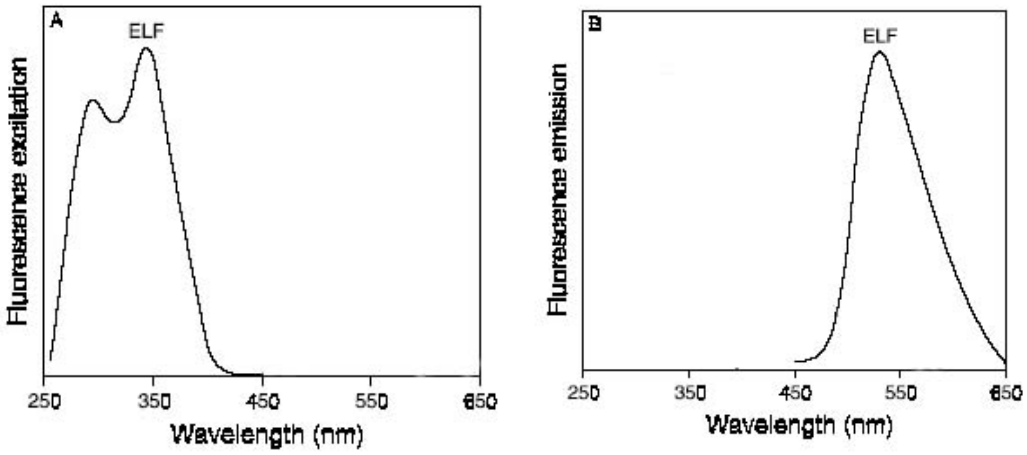

Figure 4.1. (A) The normalized excitation spectra of the ELF 97 alcohol precipitate (ELF). (B) The normalized emission spectra of ELF 97 alcohol precipitate (Molecular Probes, Inc. 2001).

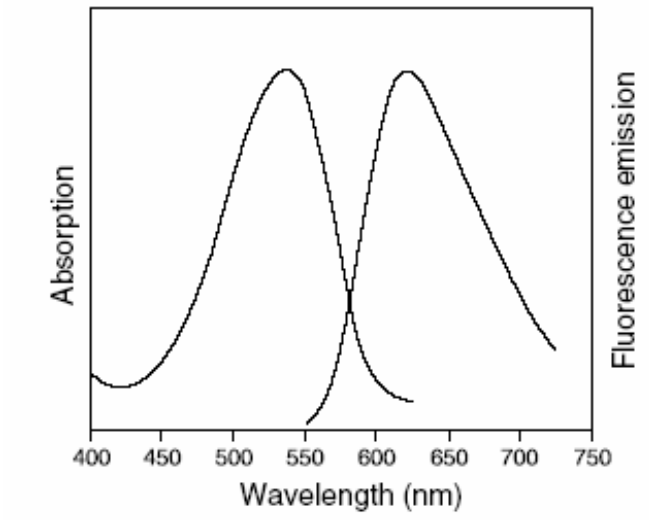

Figure 4.2. Excitation and fluorescence emission spectra of propidium iodide (PI) bound to dsDNA (Molecular Probes, Inc. 2003). The excitation peak is around 536 nm, emission peak around 617nm.

In this study, ELF 97 phosphate was used to visualize the APase synthetic activity induced by phosphate starvation. Due to the great difference between the blue fluorescence intensity of ELF 97 APase substrate and the APase-dependent yellow-green fluorescence intensity, the biofilms were counterstained with propidium iodide (PI) to improve the contrast of APase-positive and APase–negative cells for better visual microscopic examination and photography. Since the excitation spectrum of PI dye (Figure 4.1) is well separated from that of the ELF 97 precipitate, the cells that have been probed with ELF 97 and PI can be visualized sequentially with the appropriate filter sets without fear that spectral overlap will introduce ambiguous results. PI is a nucleic acid stain which is generally excluded from viable cells (Molecular Probes, Inc. 2001). After PI counterstaining, cells with APase activity exhibit yellow-green fluorescence while cells without APase activity are red.

After 5 d of growth, the coupons were withdrawn from the drip-flow reactor. Some pieces of coupons were cut into halves using sterile scissors in the flame area to get the six samples. They were treated by ELF 97 phosphate, or PI stain, or kept for subsequent rhodamine B control counterstaining treatment according to Table 4.2.

The sample, high-P_i sample and the APase control sample were treated by 0.25 mM ELF 97 phosphate solution (Molecular Probes, Inc. 2001) in a staining container at 37 ^{o}C in the dark for 30 min. Then the ELF 97 phosphate solution was removed from the container. PI solution of 0.3 mM was added into the chambers to submerge the coupons

with the sample, the high-P_i control sample and PI counterstained control sample. The staining solution was removed from the container after 2 h.

Cryoembedding and Cryostat Sectioning

All the samples were processed by the cryoembedding and cryosectioning technology as introduced in Chapter 3. Cross sections, 5-µm-thick, were collected on slides for microscopic examination.

Microscopic Examination

The ELF 97 alcohol precipitate exhibits a fluorescence emission that is separated from its excitation wavelength by greater than 100 nm (Figure 4.1). The difference between the excitation and emission wavelengths of most endogenous fluorescent components is usually much less, making the ELF 97 signal clearly distinguishable from the inherent autofluorescence of the sample (Molecular Probes, Inc. 2001).

For image analysis, biofilm sections were counterstained with 1 mg/l rhodamine B (Huang *et al.*, 1998). After rhodamine B counterstaining all the cells with APase and cells without APase would emit red fluorescence while only cells with APase emit yellow-green fluorescence. Prior to microscopic observation, about 30 µl of 1 µg/l rhodamine B solution was pipetted onto the mounted cryosections of the sample, the high-P_i control

sample, and the rhodamine B counterstained control sample (Table 4.2) and left for 1 min. The stain solution was drained by tilting the slides. The samples were then air dried for 5 min.

The cross sections were examined using a Nikon Eclipse E800 light microscope. The yellow-green fluorescence emitted by the ELF 97 precipitate was visualized by an ELF 97 filter cubic unit equipped with an excitation filter (wavelength, 360 nm), a dichroic mirror (model, DM-400), and a 520—560 nm bandpass emission filter (wavelength, 540 nm). A TRITC filter set containing an excitation filter (wavelength, 540 nm), a dichroic mirror (model, DM-565), and a emission filter (wavelength, 630 nm) was set to capture the red fluorescence from PI / rhodamine B (red) (the excitation peak is around 536 nm, emission peak around 617 nm) (Figure 4.1). A 10× dry lens was used.

Image Analysis by MetaMorph Software

Quantitative image analysis was performed using the built-in Linescan function in MetaMorph image analysis software as described in Chapter 3.

Table 4.2. Pretreatment of the drip-flow reactor biofilms prior to microscopic examination of APase expression

	Sample	High-P_i Control Sample	Control Sample	APase Control Sample	PI Counterstained Control Sample	Rhodamine B Counterstained Control Sample
ELF 97 phosphate	30 min	30 min	——	30 min	——	——
PI counterstaining	2 h	2 h	——	——	2 h	——
Rhodamine B	1 min	1 min	——	——	——	1 min

Results

In this study, biofilms ranged from 36 to 106 μm thick with a mean thickness of 60.0 ± 19.4 μm were obtained, on average thinner than those grown for the study in Chapter 3. Under the illustration of UV light, weak blue fluorescence emitted from the ELF 97 phosphate was detected throughout the biofilms (data not shown). It indicated ELF 97 phosphate could penetrate into the deep biofilms. The control sample without staining and the PI control sample without ELF 97 staining did not show yellow-green fluorescence. ELF 97 phosphate substrate was unavailable for APase, and negligible inherent autofluorescence of the sample would be captured by the 520—560 nm bandpass emission filter due to the great difference between the excitation wavelength and emission wavelength of ELF 97 precipitate. The high-P_i control sample with continuous high-P_i medium showed no APase activity, indicating that phosphate starvation was required to induce the APase expression (Figure 4.2)

After 16 h of exposure to the P_i-deficient Keck project medium, the biofilm samples developed the enzyme-labeled fluorescence and revealed a distinct, thin APase expression band near the biofilm-bulk fluid interface indicating the heterogeneous spatial patterns of APase expression (Figure 4.3A, C, F). Furthermore, APase activity was found to be localized as many distinct but sparse bright spots with fluorescent ELF 97

precipitate which was dispersed inside the biofilm, shown by the overlay of transmitted-light image and APase activity image (Figure 4.3 C). This indicated the some local APase activity deep in the biofilms, yet the mechanisms are not currently understood.

Linescanning was applied at individual spots with different total biofilm thickness to reveal the APase expression related to the biofilm thickness (Figure 4.5). As introduced in Chapter 3, APase activity zone was determined from the span of the enzyme-labeled fluorescence peak near the biofilm-bulk fluid interface, the total biofilm thickness ($L_{biofilm}$) from rhodamine B counterstaining.

In thick biofilms, we could generally tell that the thicker the biofilm, the sharper the peak of ELF 97 fluorescence and the flatter and longer the shoulder. This trend was not evident in thin biofilms.

Linescans were located at 17 spots to quantify the dimensions of APase activity zone in biofilm cross sections, L_{APase}, of different thicknesses (Figure 4.6). Individual measurements of L_{APase} varied, ranging from approximately 5.0 to approximately 17.8 μm with a mean value of 11.9 ± 3.7 μm. Most of APase activity was concentrated on the top 12 μm of the biofilm, about one-fifth of the total biofilm thickness.

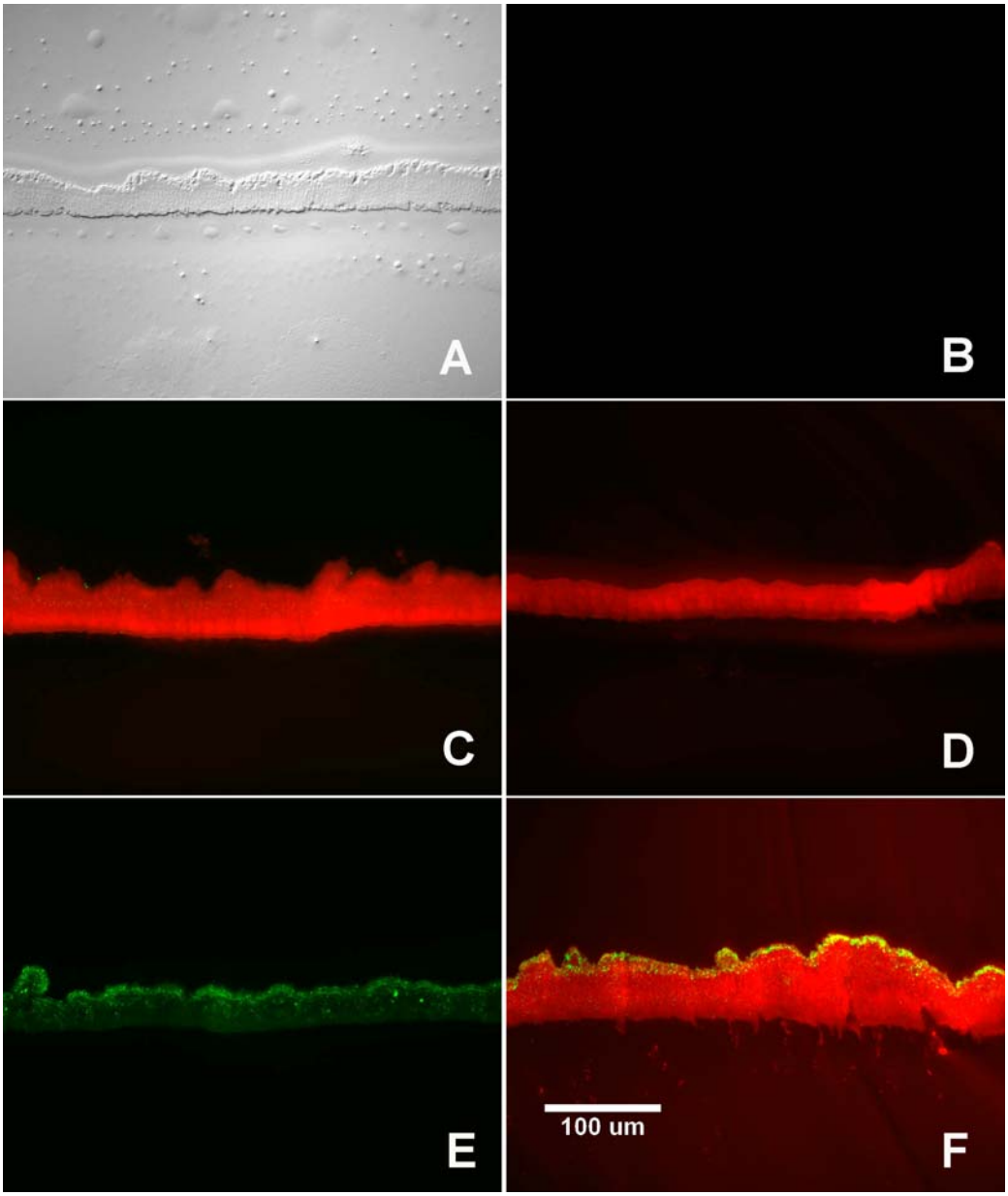

Figure 4.3. Nikon light microscopic images showing the spatial patterns of APase activity expressed during phosphate starvation in the control samples and the sample of *P. aeruginosa* PAO1 (pAB1) biofilm cross sections: (A) transmitted-light image of control sample without staining; (B) color-combined image of the control sample without staining; (C) color-combined image of High-P_i control sample stained with ELF 97 and counterstained with PI and rhodamine B; (D) color-combined image of PI control sample stained by PI; (E) color-combined image of ELF 97 control sample stained by ELF 97 phosphate; (F) sample showing the spatial patterns of APase expression in sectioned *P. aeruginosa* PAO1 (pAB1) biofilms induced by phosphate starvation for 16 h and then stained by ELF 97 phosphate (yellow-green) and counterstained by rhodamine B (red). The images are oriented with the substrata at the bottom of the pictures.

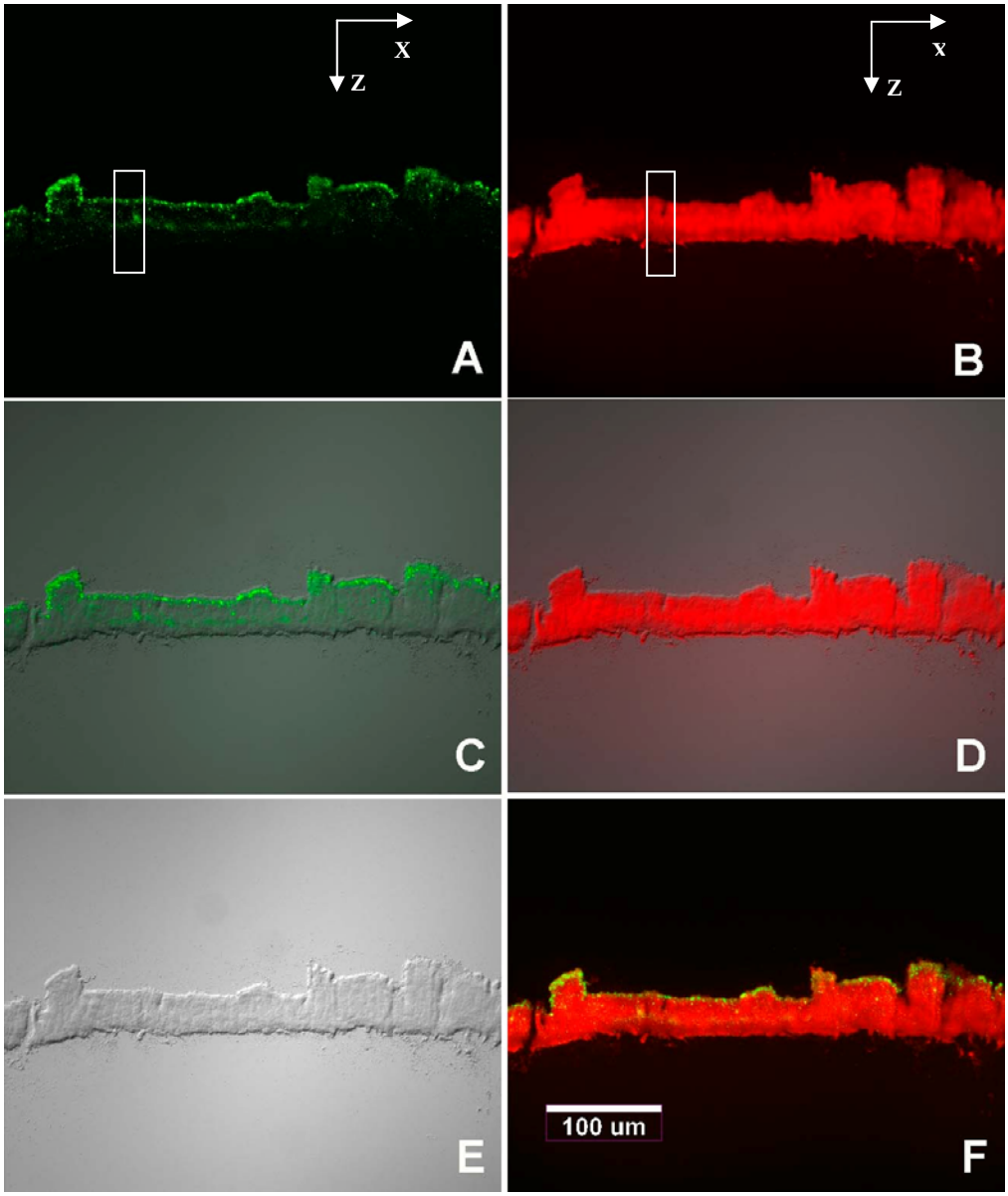

Figure 4.4. Nikon light microscopic images showing the spatial patterns of APase expression in *P. aeruginosa* PAO1 (pAB1) biofilm cross sections sampled after 16 h of phosphate starvation. (A) APase activity labeled by fluorescence from the ELF 97 precipitate which was captured by an ELF 97 filter set (yellow-green); (B) Biomass distribution visualized by fluorescence from rhodamine B counterstaining which was captured by a TRITC filter set (red). Rhodamine B stained area represents the total biomass; (C) Overlay of transmitted-light image and APase activity image; (D) Overlay of transmitted-light image and rhodamine B stained biomass image; (E) Transmitted-light image; (F) Color-combined image of the sample stained by ELF 97 phosphate and counterstained by rhodamine B. The images are oriented with the substrata at the bottom of the pictures. The white boxes are set at representative locations to show linescanning in this study as described in Chapter 3.

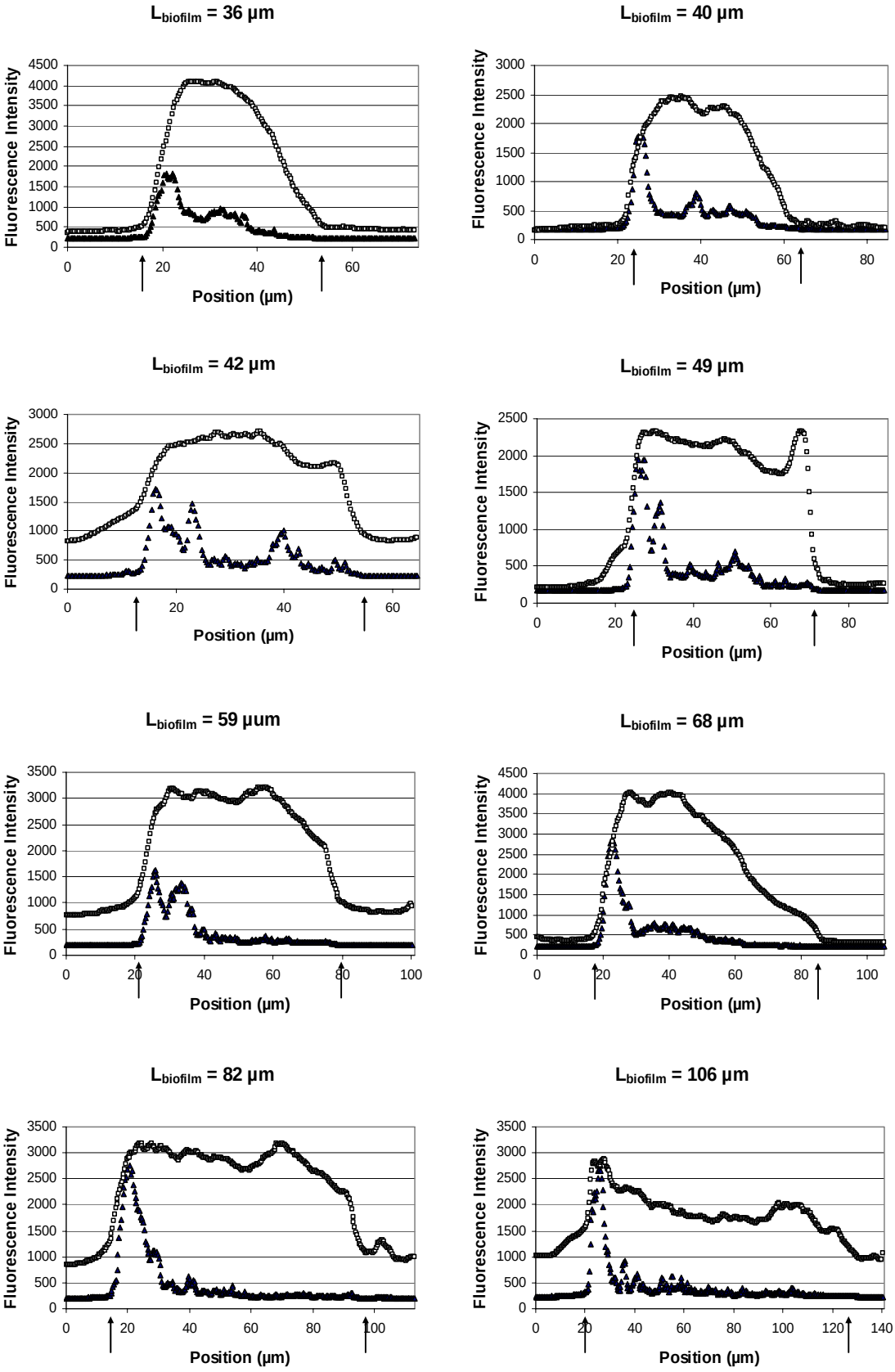
$L_{biofilm}$ = 36 µm
Fluorescence Intensity
Position (µm)
$L_{biofilm}$ = 40 µm
Fluorescence Intensity
Position (µm)
$L_{biofilm}$ = 42 µm
Fluorescence Intensity
Position (µm)
$L_{biofilm}$ = 49 µm
Fluorescence Intensity
Position (µm)
$L_{biofilm}$ = 59 µum
Fluorescence Intensity
Position (µm)
$L_{biofilm}$ = 68 µm
Fluorescence Intensity
Position (µm)
$L_{biofilm}$ = 82 µm
Fluorescence Intensity
Position (µm)
$L_{biofilm}$ = 106 µm
Fluorescence Intensity
Position (µm)

Figure 4.5. Profiles of APase activity along the linear transects across the sectioned *P. aeruginosa* PAO1 (pAB1) biofilms of different thicknesses obtained by the Linescan analysis. The position axis represents the linear transect across the biofilm in the Z dimension shown in Figure 4.4A, B. In each panel, the first arrow points to the biofilm-bulk fluid interface, the second one to the substratum. ▲, APase; □, rhodamine B stained biomass. $L_{biofilm}$: total biofilm thickness.

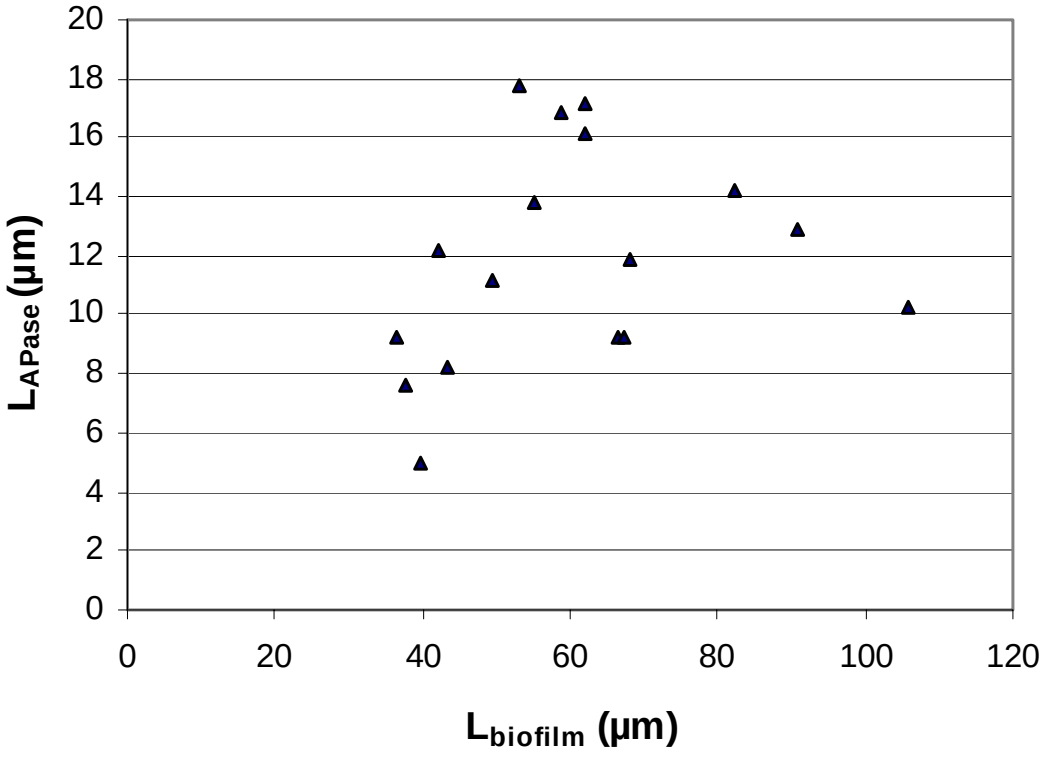

Figure 4.6. The dimension of APase expression zone in different-depth biofilm cross sections. L_{APase}: dimension of the zone of APase expression, indicated by the span of the APase activity peak close to the biofilm-bulk fluid interface; $L_{biofilm}$: total biofilm thickness.

In 5-d *P. aeruginosa* PAO1 (pAB1) biofilms, individual ratios of thickness of APase expression zone to the total biofilm thickness, $L_{APase}/L_{biofilm}$, ranged from 0.10 to 0.34 and fluctuated around 0.21 with a standard deviation of 0.07. The ratios fluctuated significantly with increasing biofilm thicknesses. However, the points were distributed more randomly in thin biofilms. These have been directly shown by the individual profiles of APase expression in Figure 4.5.

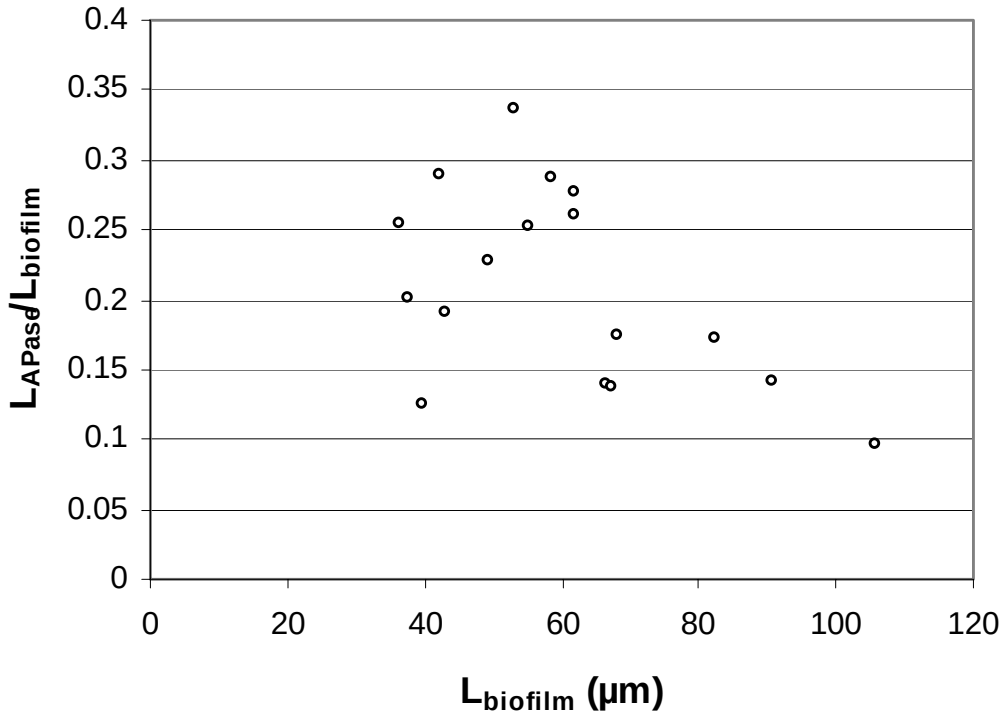

Figure 4.7. The ratio of thickness of APase expression zone to the total biofilm thickness with respect to different-depth biofilm cross sections.

Discussion

In this study, heterogeneous spatial patterns of APase expression were visualized by the enzyme-labeled fluorescence induced by 16 h of phosphate starvation. A distinct APase-positive band was revealed near the biofilm-bulk fluid interface. APase activity was also found to be localized as many distinct but sparse bright spots with fluorescent ELF 97 precipitate which was dispersed inside the biofilm.

The findings of heterogeneous APase expression within these *P. aeruginosa* biofilms are basically consistent with those obtained by Huang *et al.* (1998) and Xu *et al.* (1998): a distinct spatially non-uniform pattern of APase expression which appeared as a sharply delineated band of APase activity. Huang *et al.* reported that the band of APase activity represented only approximately one-sixth of the total biofilm thickness. Xu *et al.* obtained a mean ratio $L_{APase}/L_{biofilm}$ of about 0.26 where the mean dimension of APase activity bands was approximately 30 μm when biofilms were grown in ambient air.

All these findings further supported the hypothesis of oxygen limitation. The whole biofilm experienced phosphate starvation after exposure to low phosphate medium. Lack of phosphate could induce the expression of alkaline phosphatase in the presence of active protein synthesis in the cells. However, the cells deep in the biofilm had less access to oxygen than the cells in the upper layer, which may result in the failure to grow

and synthesize the proteins. Alkaline phosphatase expression is therefore turned off in the depth of biofilm.

As hypothesized by Huang *et al.* (1998) and Xu *et al.* (1998), the zone of APase activity induced with phosphate starvation was determined by oxygen limitation rather than glucose limitation, which is based on the known growth stoichiometry of *P. aeruginosa* cultures and the previous findings that there are oxygen concentration gradients in similar biofilms (de Beer *et al.* 1994). Xu *et al.* measured the dissolved oxygen profile within *P. aeruginosa* biofilms in the region from the biofilm-bulk fluid interface to a point approximately 40 μm above the substratum and found the band of APase expression in the upper region of biofilm coincided with dissolved-oxygen concentrations of greater than 0.05 mg/l (Xu *et al.*, 1998).

CHAPTER 5

SPATIAL PATTERNS OF VIABILITY VISUALIZED IN *PSEUDOMONAS AERUGINOSA* DRIP-FLOW REACTOR BIOFILMS

Introduction

The previous three chapters about GFP expression revealed the heterogeneous spatial growth patterns within *P. aeruginosa* biofilms using protein expression and suggested the relationship of the spatial heterogeneity with oxygen limitation. To further reveal the heterogeneous growth patterns, a cell viability assay was performed in this work. Hope and Wilson studied the spatial distribution of viable and nonviable bacteria in hydrated microcosm dental plaques by viability profiling. They discovered an outer layer of viable bacteria surrounding an internal core of nonviable bacteria (Hope and Wilson, 2003), and found proportionally more viable bacteria in the outer layer than the lower regions of the biofilm (Hope *et al.*, 2002). The findings of the spatial patterns of GFP expression within *P. aeruginosa* biofilms (Chapter 2 and Chapter 3) were qualitatively consistent with this distribution of viable and nonviable bacteria in oral biofilms. The purpose of the work in this chapter was to determine the profile of cell viability within

the *P. aeruginosa* biofilms, which would provide information to reveal the relationship of spatial physiological heterogeneity to cell viability patterns.

Conventional direct-count assays of bacterial viability are based on metabolic characteristics or membrane integrity. However, methods relying on metabolic characteristics often only work for a limited subset of bacterial groups (Kaprelyants and Kell, 1992) and methods for assessing bacterial membrane integrity commonly have high levels of background fluorescence (Davies, 1991). Both types of determinations suffer from being very sensitive to growth and staining conditions (Brunius, 1980; McFeters *et al.*, 1991). Because of the marked differences in morphology, cytology and physiology among the many bacterial genera, a universally applicable direct-count viability assay has been very difficult to achieve (Molecular Probes, Inc. 2003)

In this study, the LIVE/DEAD *Bac*Light™ Bacterial Viability stain was applied to determine the spatial distribution of viable and dead cells in *P. aeruginosa* biofilms by fluorescence assay. Component A (SYTO 9), a green-fluorescent nucleic acid stain and component B (PI)), a red-fluorescent nucleic acid stain, can be either mixed or applied separately. When used alone, the SYTO 9 stain generally labels all bacteria in a population — those with intact membranes and those with damaged membranes. In contrast, PI penetrates only bacteria with damaged membranes, causing a reduction in the SYTO 9 stain fluorescence when both dyes are present. Thus, with an appropriate mixture of the SYTO 9 and PI stains, cells with intact cell membranes stain fluorescent green, whereas cells with damaged membranes stain fluorescent red. The

excitation/emission maxima for these dyes are about 480/500 nm for SYTO 9 stain and 490/635 nm for PI (Figure 4.2). The background remains virtually non-fluorescent (Molecular Probes, Inc. 2003).

Systematic errors may happen in LIVE/DEAD *Bac*Light bacterial viability assays. A common criterion for bacterial viability is the ability of a bacterium to reproduce in suitable nutrient medium. Exponentially growing cultures of bacteria typically yield results with the LIVE/DEAD *Bac*Light bacterial viability assay that correlate well with growth assays in liquid or solid media. Under certain conditions, however, bacteria having compromised membranes may be able to recover and reproduce — such bacteria may be scored as "dead" in this assay. Conversely, some bacteria with intact membranes may be unable to reproduce in nutrient medium, and yet these may be scored as "alive" (Roszak and Colwell, 1987).

Materials and Methods

Strains, Plasmids and Media

P. aeruginosa PAO1 (pAB1) strain was grown in regular Keck project medium (Table 1.1) as described in Chapter 1.

Cultivation Procedure

PAO1 (pAB1) biofilms were grown on coupon surfaces for 5 d with Keck project medium dripping at ambient temperature (23°C) as described in Chapter 3.

Sampling and Preprocessing

After 5 d of growth, the four mature biofilm samples on the coupons were treated separately by SYTO 9 or PI counterstaining (Table 5.1). The LIVE/Dead® *Bac*Light™ Bacterial Viability Kit L-7012 available through Molecular Probes, Inc. was used. 15 µl of component A (SYTO 9 stain) and 15 µl of component B (PI) were mixed in 1 ml of filter-sterilized water to stain the sample. For separate use, 15 µl of SYTO 9 or PI solution from the Kit was directly diluted in 1 ml filter-sterilized water.

Table 5.1. LIVE/DEAD *Bac*Light bacterial viability stain pretreatment of the drip-flow reactor biofilms prior to microscopic examination of viability pattern

	Sample	Control Sample	SYTO 9 Stained Control Sample	PI Counterstained Control Sample
SYTO 9 staining	2 h	——	2 h	——
PI counterstaining	2 h	——	——	2 h

The coupons were removed from the reactor channels. The SYTO 9 stained control sample was stained by SYTO 9 stain solution for 2 h, the PI counterstained control

sample stained by PI stain solution for 2 h, the sample stained by 1: 1 mixture of SYTO 9 and PI stain solution for 2 h. The liquid was removed from the staining container after staining. Then all the samples were ready for cryoembedding.

Cryoembedding and Cryostat Sectioning

Cryoembedding and cryosectioning technology was applied as introduced in Chapter 3. Biofilm cross sections, 5-μm-thick, were mounted on the slides for microscopic examination.

Microscopic Examination

The cross sections were examined using a Nikon Eclipse E800 light microscope. According to the excitation and emission spectra of SYTO 9 and PI (Figure 4.2), a FITC filter block containing an exciter (wavelength of 465-495 nm), a dichroic mirror (model DM-505), and an emitter (wavelength of 515-555 nm) was set for SYTO 9 fluorescence (green). A TRITC filter block containing an exciter (wavelength of 540 nm), a dichroic mirror (model DM-565), and an emitter (wavelength of 630 nm) was set for PI fluorescence (red). A 10× dry lens was used.

Image Analysis by MetaMorph Software

Quantitative image analysis was performed using the built-in Linescan function in MetaMorph image analysis software as described in Chapter 2.

Results

Biofilms of mean thickness of 121.4 ± 22.4 μm were obtained for the present study. As shown in Figure 5.1, the control sample without staining did not show fluorescence. Panel C showed a sharp viable cells band indicated by green fluorescence of SYTO 9 stain in the control sample. It was immediately puzzling because SYTO 9 stain should generally label all bacteria in a population — those with intact membranes and those with damaged membranes when used alone.

After LIVE/DEAD *Bac*Light staining, the biofilm samples developed the two-color fluorescence and showed the heterogeneous cell viability distribution (Figure 5.2A, C, F). The occupation of PI stain at the nonviable zone reduced the SYTO 9 stain fluorescence at the same spots. Thus the green fluorescence emitted from the upper layer of the biofilms captured by FITC filter set marked the viable zone. It existed as a sharp band close to the biofilm-bulk fluid interface (Figure 5.2A, C, F). The nonviable zone stained by PI dye appeared to be very uniform throughout the biofilms (Figure 5.2B, D).

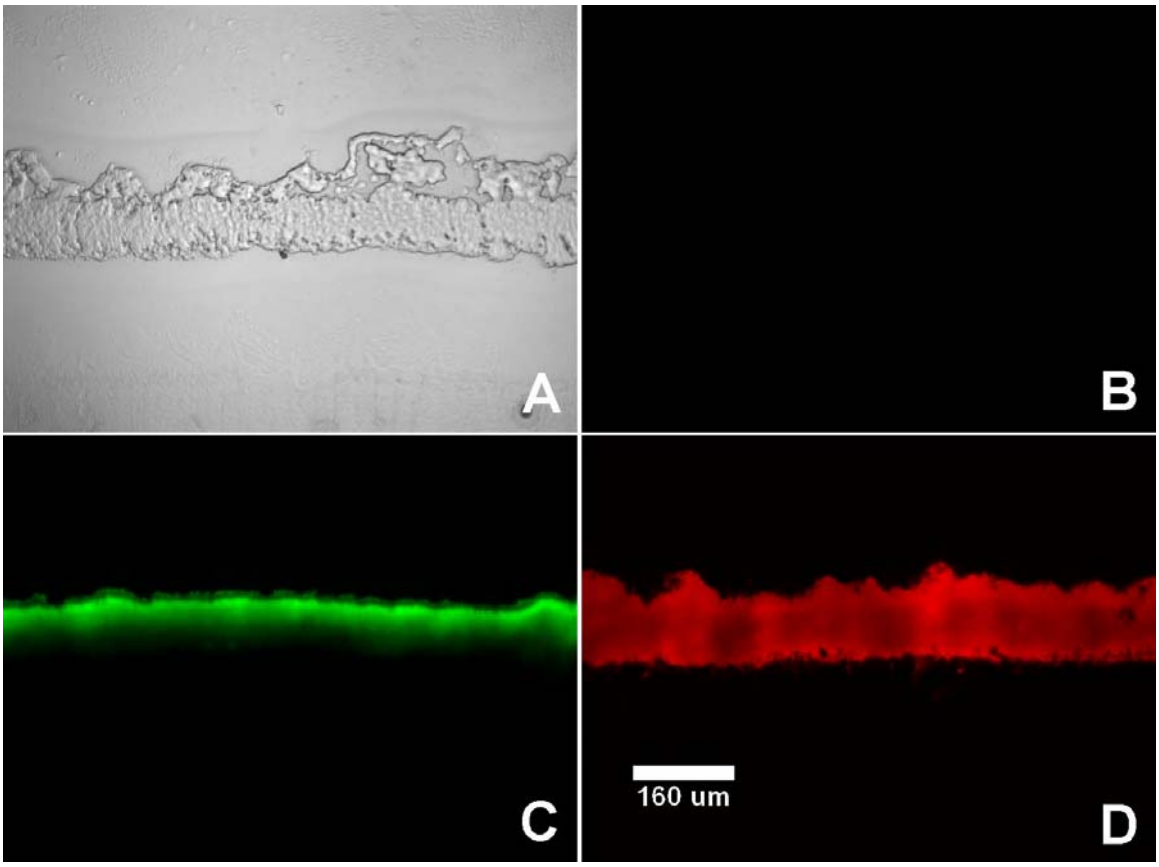

Figure 5.1. Nikon light microscopic images showing the spatial viability patterns of the control samples and the sample of *P. aeruginosa* PAO1 (pAB1) biofilm cross sections by the LIVE/DEAD *Bac*Light bacterial viability assay: (A) Transmitted-light image of control sample without staining; (B) Color-combined image of the control sample without any staining; (C) Overlay of the transmitted-light image and the color-combined image of the control sample stained only by SYTO 9; (D) Color-combined image of the control sample stained only by PI dye; The images are oriented with the substrata at the bottom of the pictures.

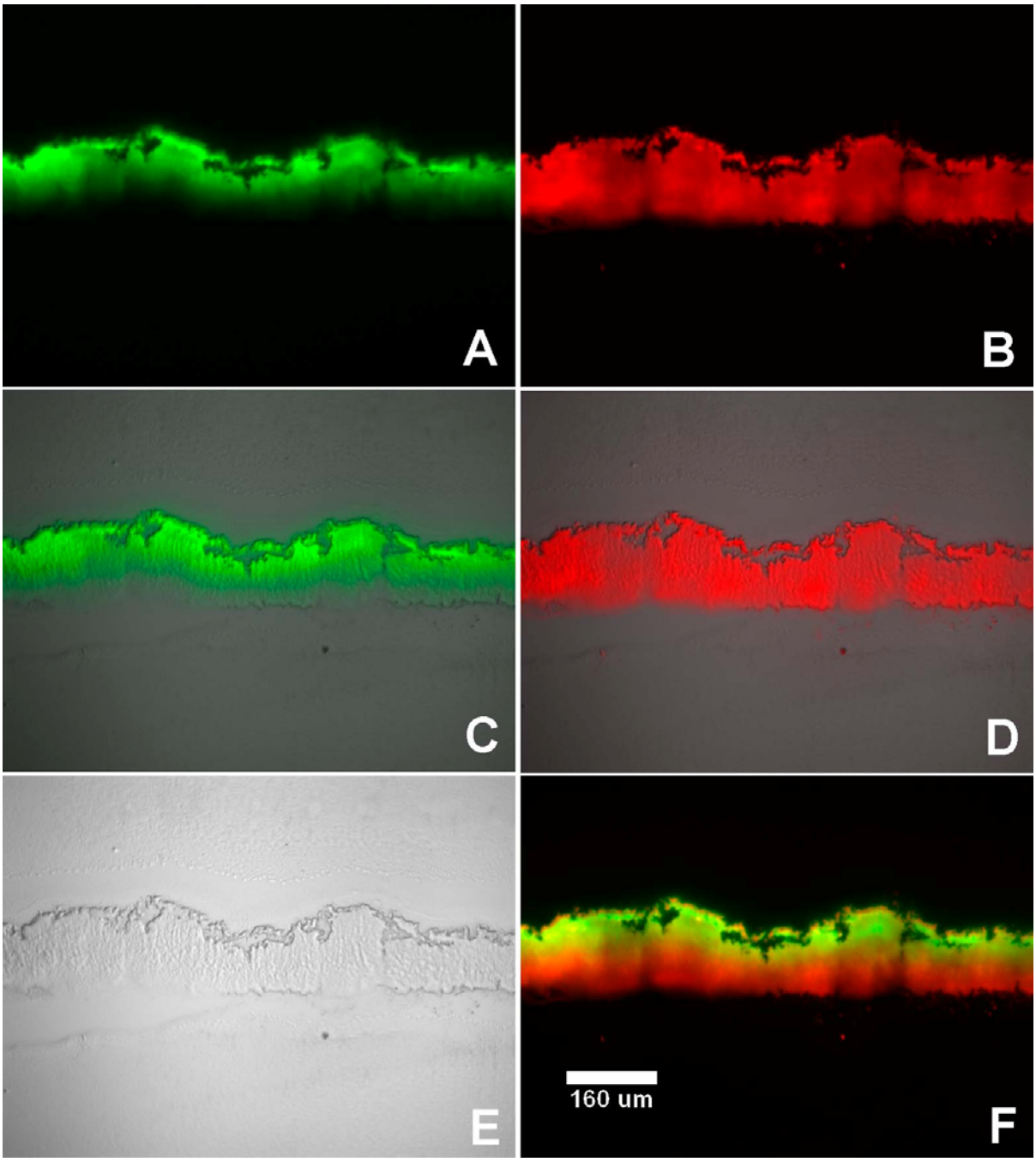
A
B
C
D
E
160 um
F

Figure 5.2. Nikon light microscopic images showing the cell viability patterns of the sectioned *P. aeruginosa* PAO1 (pAB1) biofilm samples. (A) Viable zone labeled by fluorescence from the SYTO stain which was captured by an FITC filter set (green). SYTO 9 stained area represents the live cells; (B) Nonviable zone visualized by fluorescence from PI counterstaining which was captured by a TRITC filter set (red). PI stained area represents the dead cells; (C) Overlay of transmitted-light image and viable zone image; (D) Overlay of transmitted-light image and nonviable zone image; (E) Transmitted-light image; (F) Color-combined image of the sample stained by SYTO 9 and counterstained by PI showing the cell viability distribution. The images are oriented with the substrata at the bottom of the pictures. The white boxes are set at representative locations to show linescanning in this study as described in Chapter 3.

Discussion

The LIVE/DEAD *Bac*Light bacterial viability assay showed the heterogeneous spatial patterns of the viable and nonviable cells: an outer layer of viable cells against a nonviable background in these biofilms and proportionally more viable cells located in the upper layers of biofilms than the deeper layers. All these findings correspond very well to those of Hope *et al.* (2002) obtained for oral biofilms using LIVE/DEAD bacterial viability staining in conjunction with CLSM: the upper layers of oral biofilms contain proportionally more viable bacteria than the lower regions of the biofilm.

However, as mentioned before, the images of individual STYO 9 staining threw doubt on the effectiveness of applying LIVE/DEAD *Bac*Light viability assay to *P. auruginosa* biofilms. Molecular Probes Inc. has tested the LIVE/DEAD *Bac*Light Viability Kit on *P. aeruginosa* culture. This species in planktonic culture has shown a good correlation between the results obtained with the LIVE/DEAD *Bac*Light Bacterial

Viability Kit and those obtained with standard plate counts. The test was performed on logarithmically growing cultures of the organism. The standard issued by Molecular Probes Inc. (2003) obtained from the test on the logarithmically growing planktonic cultures might not represent the situation of biofilms where most of cells are sessile and living in a steady state.

According to the standard, separate SYTO 9 staining should result in the overall green fluorescence in the cell culture including those with intact membranes and those with damaged membranes, but the biofilm sample only showed a zone stained by SYTO 9 limited on the upper layer. This discrepancy from the standard may be an artifact due to the low penetration of SYTO 9 dye into the *P. aeruginosa* biofilms. *P. aeruginosa* biofilms may impede the diffusion of SYTO 9 into the deep layer or biodegrade the SYTO 9 dye.

Thus, more tests on the application of LIVE/DEAD *Bac*Light Bacterial Viability Kit to *P. aeruginosa* biofilms should be carried out. The results could then be compared with the results of standard plate counts to tell the feasibility of applying this viability stain kit to viability study of *P. aeruginosa* biofilm. Prior to confirming the methodological validity, we can not draw the credible conclusions about the viability pattern of *P. aeruginosa* biofilms by analyzing the images so far we obtained using the LIVE/DEAD *Bac*Light Bacterial Viability Kit.

CHAPTER 6

SUMMARY

Spatial patterns of protein synthetic activity within *P. aeruginosa* biofilms were visualized, quantified, and found to be non-uniform.

P. aeruginosa PAO1 (pAB1) carries the plasmid pAB1 which was maintained in the presence of carbenicillin at a concentration of 50 μg/ml. The high energy consumption of the plasmids impedes the growth of the cells significantly. The 5-d mature *P. aeruginosa* biofilms grown in capillary reactor ranged only from 13 to 63 μm thck, while drip-flow reactor allowed us to obtain much thicker biofilms, about 36 to 220 μm. These two reactors supplemented each other to get a wider-range study.

In this study, mature biofilms were examined in situ using capillary reactor system and temporal pattern of GFP expression during 3 h of IPTG induction was visualized. GFP activity increased during IPTG induction and was ready for microscopic observation after 3 h of induction. Meanwhile, GFP activity developed faster at the surface of cell clusters than in the center. Spatial patterns of GFP expression revealed greater GFP synthetic activity evident at the surface than in the center with the air bubble activation and 3 h of IPTG induction. GFP activity was less uniform in larger clusters than in small

ones. The thicker biofilms grown in a drip-flow reactor system showed similar physiological heterogeneity: greater GFP expression in the area close to the biofilm-bulk fluid interface than in regions close to the substratum. Most GFP activity was concentrated on the top 60 μm of the biofilm, independent of the biofilm thickness, while the ratio of $L_{GFP}/L_{biofilm}$ decreased with the increasing biofilm thickness. Generally, more protein synthesis was expressed in the surface layer of biofilms.

P. aeruginosa PAO1 (pAB1) could not grow on the minimal glycerol-glutamate Keck project media anaerobically without alternative electron accepters, which made it an obligate aerobe in this case and thus favored the working hypothesis relating the physiological heterogeneity to oxygen limitation within the biofilms. This working hypothesis was further supported by phosphate starvation-induced APase expression. Since the deep-internal portions of biofilms are generally believed to experience starvation and slow growth due to nutrient limitation in a thick aging biofilm (Xu *et al.*, 1999), APase was expected to be expressed more in the deep biofilms or uniformly throughout the biofilm after 16 h of phosphate depletion. However, the findings in Chapter 4 indicated that the APase activity induced by phosphate starvation and visualized by ELF 97 phosphate substrate staining was limited to a sharp band close to the biofilm-bulk fluid interface. In this case, phosphate limitation acted as the inducing stimulus for protein expression. Oxygen limitation emerged to be a major limiting factor for protein synthetic activity. The cells in the upper layer of biofilms have easier access to nutrients and oxygen than those in deep biofilms. Oxygen may be depleted in the deep

biofilm and unavailable for protein synthetic activity, thus forming an oxygen gradient and a heterogeneous APase expression. This has been partially demonstrated by the coincidence of APase expression in the upper region of biofilm with dissolved-oxygen concentrations of greater than 0.05 mg/l (Xu *et al.*, 1998).

If one were to provide the biofilms with medium containing nitrate or nitrite, or arginine, the bacteria should be able to grow in the absence of oxygen. We could expect a heterogeneous spatial growth pattern similar to those we obtained in this work since any substrate, in this case the electron acceptor nitrate or nitrite, or arginine, is likely to have a penetration problem. However, since we could increase the concentrations of these substrates to very high levels and the substrates could probably diffuse into the deeper biofilms, more uniform patterns of activity might be obtained.

Biofilm viability assay using the LIVE/DEAD *Bac*Light bacterial viability stain showed baffling images: a green-fluorescence band close to the biofilm-bulk fluid interface stained only by SYTO 9 and a uniform PI stained area throughout the biofilms. According to the standard test results obtained from the logarithmically growing planktonic cultures, SYTO 9 can stain all the bacteria with intact or damaged membranes when used alone. These images of SYTO 9 control samples may be artifacts due to the low penetration of SYTO 9 into the *P. aeruginosa* biofilms, or biodegradability of SYTO 9 dye by these microorganisms.

The resistance mechanisms of biofilm microorganisms to antimicrobial action are complicated. The hypothesis of oxygen limitation still needs to be further confirmed. And

most likely, penetration limitation, oxygen limitation, and maybe other unknown mechanisms are cooperating together. Which one is predominant depends on the physiological status of the biofilm microorganisms, environmental conditions, etc.

REFERENCES CITED

Anderl, J. N., Franklin, M. J., and Stewart, P. S. 2000. Role of antibiotic penetration limitation in *Klebsiella pneumoniae* biofilm resistance to ampicillin and ciprofloxacin. *Appl. Environ. Microbiol.* **44:** 1818-1824.

Anwar, H., Strap, J. L., and Costerton, J. W. 1992. Establishment of aging biofilms: possible mechanism of bacterial resistance to antimicrobial therapy. *Antimicrob. Agents Chemother.* **36:**1347-1351.

Borriello, G., Werner, E., Roe, F., Kim, A. M., Ehrlich, G. D., and Stewart, P. S. 2004. Oxygen Limitation Contributes to Antibiotic Tolerance of *Pseudomonas aeruginosa* in Biofilms. *Antimicrob. Agents Chemother.* **48:** 2659-2664.

Brunius, G. 1980. Technical aspects of the use of 3',6'-diacetyl fluorescein for vital fluorescent staining of bacteria. *Curr. Microbiol.* **4:** 321-323.

Chalfie, M., Tu, Y., Euskirchen, G., Ward, W. W., and Prasher, D. C., 1994. Green fluorescent protein as a marker for gene expression. *Science*. **263:** 802-805.

Costerton, J. W., Cheng, K.-J., Geesey, G. G., Ladd, T. I., Nickel, J. C., Dasgupta, M., and Marrie, T. J. 1987. Bacterial biofilms in nature and disease. *Ann. Rev. Microbiol.* **41:** 435-464.

Costerton, J. W., Lewandoski, Z. Caldwell, D. E., Korber, D. R., and Lappin-Scott, H. M. 1995. Microbial biofilm. *Annu. Rev. Microbiol.* **49:** 711-745.

Costerton, J. W., Stewart, P. S., Greenberg, E. P. 1999. Bacterial biofilms: A common cause of persistent infections. *Science.* **284:** 1318-1322.

Davies, C. M. 1991. A comparison of fluorochromes for direct viable counts by image analysis. *Lett. Appl. Microbiol.* **13:** 58-61.

de Beer, D., Stoodley, P., Roe, F., and Lewandowski, Z. 1994. Effects of biofilms structures on oxygen distribution and mass transport. *Biotechnol. Bioeng.* **43:** 1131-1138.

de Beer, D., Stoodley, P., and Lewandowski, Z. 1997. Measurements of local diffusion coefficients in biofilms by microinjection and confocal microscopy. *Biotechnol. Bioeng.* **53:** 151-158.

Deziel, E., Comeau, Y., Villemur, R. 2001. Initiation of biofilm formation by *Pseudomonas aeruginosa* 57RP correlates with emergence of hyperpiliated and highly adherent phenotypic variants deficient in swimming, swarming, and twitching motilities. *J. Bacteriol.* **183:** 1195-1204

Figurski, D., and Helinski, D. R. 1979. Replication of an origin-containing derivative of plasmid RK2 dependent on a plasmid function provided in *trans*. *Proc. Natl. Acad. Sci. USA.* **76:** 1648-1652.

Franklin, M. J., Chitnis, C. E., Gacesa, P., Sonesson, A., White, D. C., and Ohman, D. E. 1994. *Pseudomonas aeruginosa algG* is a polymer level alginate C5-mannuronan epimerase. *J. Bacteriol.* **176:** 1821-1830.

Franklin, M. J., and Ohman, D. E. 1993. Identification of *algF* in the *Pseudomonas aeruginosa* alginate biosynthetic gene cluster which is required for alginate O acetylation. *J. Bacteriol.* **175:** 5057-5065.

Franklin, M. J., and Ohman, D. E. 1996. Identification of *algI* and *algJ* in the *Pseudomonas aeruginosa* alginate biosynthetic gene cluster which are required for alginate O acetylation. *J. Bacteriol.* **178:** 2186-2195.

Harowitz, A., Krichevsky, M. J., and Atlas, R. M., 1983. Characteristics and diversity of subartic marine oligotrophic, stenoheterotrophic, and euryheterotrophic bacterial populations, *Can. J. Microbiol.* **29:**527-535.

Heim, R., Prasher, D. C., and Tsien, R. Y., 1994. Wavelength mutations and posttranslational autoxidation of green fluorescent protein. *Proc. Natl. Acad. Sci. USA.* **91:**12501-12504.

Hope, C. K., Clements, D., and Wilson, M. 2002. Determining the spatial distribution of viable and nonviable bacteria in hydrated microcosm dental plaques by viability profiling. *J. Appl. Microbiol.* **93:** 448-455.

Hope, C. K. and Wilson, M. 2003. Measuring the thickness of an outer layer of viable bacteria in an oral biofilm by viability mapping. *J. Microbiol. Methods.* **54:** 403-410.

Hou, C. I. Gronlund, A. F., and Campbell, J. J. R. 1966. Influence of phosphate starvation on cultures of *Pseudomonas aeruginosa*. *J. Bacteriol.* **92:** 851-855.

Huang, C.-T., Xu, K. D., McFeters, G. A., and Stewart, P. S. 1998. Spatial patterns of alkaline phosphatase expression within bacterial colonies and biofilms in response to phosphate starvation. *Appl. Environ. Microbiol.* **64:** 1526-1531.

Kaprelyants, A. S, and Kell, D. B. 1992. Rapid assessment of bacterial viability and vitality by rhodamine 123 and flow cytometry. *J. Appl. Bacteriol.* **72:** 410-422.

Madigan, M. T., Martinko, J. M., Parker, J. 2003. Brock Biology of Microorganisms. p. 370. Pearson Education, Inc., New Jersey.

Mallette, M. F., Cowan, C. I. and Campbell, J. J. R. 1964. Growth and survival of *Escherichia coli* in medium limited in phosphate. *J. Bacteriol.* **87:**779-785.

McFeters, G. A., Singh, A. Byun, S., Callis, P. R., and Williams, S. 1991. Acridine orange staining reaction as an index of physiological activity in *Escherichia coli*. *J. Microbiol. Methods.* **13:** 87-97.

McLean, R. J. C. and Decho, A. W. 2002. Molecular ecology of biofilms. p. 1. Horizon Scientific Press. Norfolk.

Moat, A. G., Foster, J. W., Spector, M. P. 2002. Microbial physiology. (4^{th} ed.), Wiley-Liss, Inc. New York.

Molecular Probes, Inc. 2001. ELF 97 Immunohistochemistry Kit Product Information.

Molecular Probes, Inc. 2003. LIVE/DEAD *Bac*Light™ Bacterial Viability Kits Product Information.

Molecular Probes, Inc. 2003. Propidium Iodide Nucleic Acid Stain Product Information.

Molecular Probes, Inc. 2003. SYTO Green-Fluorescent Nucleic Acid Stain Product Information.

Murga, R., Stewart, P. S., and Daly, D. 1994. Quantitative analysis of biofilm thickness variability. *Biotechnol. Bioeng.* **45:** 503-510.

Nivens, D. E., Ohman, D. E., Williams, J., and Franklin, M. J. 2001. Role of alginate and its O acetylation in formation of *Pseudomonas aeruginosa* microcolonies and biofilms. *J. Bacteriol.* **183:** 1047-1057.

O'Toole, G. A. and Kolter, R. 1998. Flagellar and twitching motility are necessary for *Pseudomonas aeruginosa* biofilm development. *Mol. Microbiol.* **30:** 295-304.

Prasher, D. C., Eckenrode, V. K., Ward, W. W., Prendergast, F. G., Cormier, M. J., 1992. Primary structure of the aequorea-victoria green-fluorescent protein. *Gene.* **111:** 229-233.

Rashid, M. H., and A. Kornberg. 2000. Inorganic polyphosphate is needed for swimming, swarming, and twitching motilities of *Pseudomonas aeruginosa*. *Proc. Natl. Acad. Sci.* **97:** 4885-4890.

Roszak, D. B., and Colwell, R. R. 1987. Survival strategies of bacteria in the natural environment. *Micorbiol. Rev.* **51:** 365-379.

Shigeta, M., H. Komatsuzawa, M. Sugai, H. Suginaka, and T. Usui. 1997. Effect of the growth rate of *Pseudomonas aeruginosa* biofilms on the susceptibility to antimicrobial agents. *Chemotherapy (Basel)* **43:**137-141.

Stewart, P. S. 1996. Theoretical aspects of antibiotics diffusion into microbial biofilms. *Antimicrob. Agents Chemother.* **40:** 2517-2522.

Stewart, P. S. 2003. Diffusion in biofilms. *J. Bacteriol.* **185:** 1485-1491.

Sternberg, C., Christensen, B. B., Johansen, T., Nielsen, A. T., Andersen, J. B., Givskov, M., and Molin, S. 1999. Distribution of bacterial growth activity in flow-chamber biofilms. *Appl. Environ. Microbiol.* **65:** 4108-4117.

Stoodley, P., de Beer, D., and Lewandowski, Z. 1994. Liquid flow in biofilm systems. *Appl. Environ. Microbiol.* **60:** 2711-2716.

Tanaka,G., Shigeta, M., Komatsuzawa, H., Sugai,M. Suginaka, H. and Usui T. 1999. Effect of the Growth Rate of *Pseudomonas aeruginosa* Biofilms on the Susceptibility to Antimicrobial Agents: β-Lactams and Fluoroquinolones. *Chemotherapy (Basel).* **45:** 28-36.

Walters, M. C., Roe, F., Bugnicourt, A., Franklin, M. J., Stewart, P. S. 2003. Contributions of antibiotic penetration, oxygen limitation, and low metabolic activity to tolerance of *Pseudomonas aeruginosa* biofilms to ciprofloxacin and tobramycin. *Antimicrob. Agents Chemother.* **47:** 317-323

Wentland, E. J., Stewart, P. S., Huang, C.-T., McFeters, G. A. 1996. Spatial variations in growth rate within *Klebsiella pneumoniae* colonies and biofilm. *Biotechnol. Prog.* **12:** 316-321.

West, S. E., Schweizer, H. P., Dall, C., Sample, A. K., and Runyen-Janecky, L. J. 1994. Construction of improved *Escherichia-Pseudomonas* shuttle vectors derived from pUC18/19 and sequence of the region required for their replication in *Pseudomonas aeruginosa. Gene*. **148:** 81-86.

Wilson T. 1990. Confocal Microscopy. London: Academic.

Xu, K. D. 1999. Physiological heterogeneity and starvation in mature *Pseudomonas aeruginosa* biofilms. Ph.D. thesis, Montana State University-Bozeman, Montana.

Xu, K. D., Stewart, P. S., Xia, F., Huang, C.-T., and McFeters, G. A. 1998. Spatial physiological heterogeneity in *Pseudomonas aeruginosa* biofilm is determined by oxygen availability. *Appl. Environ. Microbiol.* **64:** 4035-4039

Yu, F., G. M. Callis, and Stewart, P. S. 1994. Cryosectioning of biofilm for microscopic examination. *Biofouling* **8:** 85-91.